Inorganic Chemistry

Article

pubs.acs.org/IC

Solventless Supramolecular Chemistry via Vapor Diffusion of Volatile Small Molecules upon a New Trinuclear Silver(I)-Nitrated Pyrazolate Macrometallocyclic Solid: An Experimental/Theoretical Investigation of the Dipole/Quadrupole Chemisorption Phenomena

Rossana Galassi,*[,†] Simone Ricci,[†] Alfredo Burini,*[,†] Alceo Macchioni,[‡] Luca Rocchigiani,[‡] Fabio Marmottini,[§] Sammer M. Tekarli,[⊥] Vladimir N. Nesterov,[⊥] and Mohammad A. Omary*[,⊥]

[†]School of Science and Technology, University of Camerino, Via Sant'Agostino 1, Camerino I-62032, Italy

[‡]Dipartimento di Chimica, Università di Perugia, Via Elce di Sotto, Perugia I-06123, Italy

[§]Dipartimento di Ingegneria Civile ed Ambientale, Università di Perugia, Via G. Duranti, Perugia I-06123, Italy

[⊥]Department of Chemistry, University of North Texas, Denton, Texas 76203, United States

Supporting Information

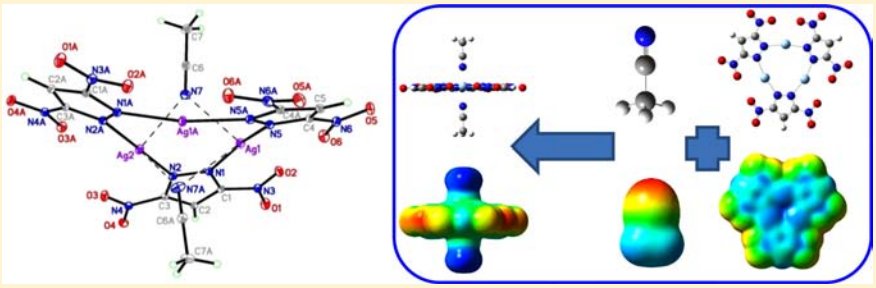

ABSTRACT: A comparative study on the tendency of a new trinuclear silver(I) pyrazolate, namely, [*N*,*N*-(3,5-dinitropyrazolate)Ag]$_3$ (**1**), and a similar compound known previously, [*N*,*N*-[3,5-bis(trifluoromethyl)pyrazolate]Ag]$_3$ (**2**), to adsorb small volatile molecules was performed. It was found that **1** has a remarkable tendency to form adducts, at room temperature and atmospheric pressure, with acetone, acetylacetone, ammonia, pyridine, acetonitrile, triethylamine, dimethyl sulfide, and tetrahydrothiophene, while carbon monoxide, tetrahydrofuran, alcohols, and diethyl ether were not adsorbed. On the contrary, **2** did not undergo adsorption of any of the aforementioned volatile molecules. Adducts of **1** were characterized by elemental analysis, IR, thermogravimetric analysis (TGA), Brunauer–Emmett–Teller (BET) surface area, and diffusion NMR measurements. The crystal structures of **1**·2CH_3CN and compound **3**, derived from an attempt to crystallize the adduct of **1** with ammonia, were determined by single-crystal X-ray diffractometric studies. The former shows a sandwich structure with a 1:2 stoichiometric [Ag_3]/[CH_3CN] ratio in which one acetonitrile molecule points above and the other below the centroid of the Ag_3N_6 metallocycle. Compound **3** formed via rearrangement of the ammonia adduct to yield an anionic trinuclear silver(I) derivative with an additional bridging 3,5-dinitropyrazolate and having $[Ag(NH_3)_2]^+$ as the counterion, $[Ag(NH_3)_2][N,N\text{-}(3,5\text{-dinitropyrazolate})_4Ag_3]$. Irreversible sorption and/or decomposition upon vapor exposure are desirable advantages toward toxic gas filtration applications, including ammonia inhalation. TGA confirms the analytical data for all of the samples, showing weight loss for each adsorbed molecule at temperatures significantly higher than the corresponding boiling temperature, which suggests a chemical-bonding nature for adsorption as opposed to physisorption. BET surface measurements of the "naked" compound **1** excluded physical adsorption in its porous cavities. Density functional theory simulation results are also consistent with the chemisorption model, explain the experimental adsorption selectivity for **1**, and attribute the lack of similar adsorption by **2** to significantly less polarizable electrostatic potential and also to strong argentophilic bonding whose energy is even higher than the quadrupole–dipole adduct bond energy upon proper selection of the density functional.

INTRODUCTION

Cyclic trinuclear complexes of monovalent coinage metals represent an emerging class of compounds with intriguing features in the fields of acid–base chemistry,[1] supramolecular assembly,[2] and metalloaromaticity.[3] These compounds have found application in high-performance optoelectronic devices[4] because of their photophysical properties.[5] Tekarli et al. described that the π-acid–base properties and cation–π interactions involving such coinage metal metallocycles are governed by the nature of the bridging ligand, ligand substituents, and/or metal center. They reported a π-acidity

Received: July 29, 2013
Published: November 20, 2013

order increasing in the directions gold(I) < copper(I) < silver(I) for the metal center, imidazolate < carbeniate < pyrazolate < triazolate for the bridging ligand, and 3,5-dimethylpyrazolate < pyrazolate < 3,5-bis(trifluoromethyl)-pyrazolate for the substituents on an example pyrazolate ligand.[6] Afterward, the synthesis of a π-acid metallocycle can be designed by choosing a bridging pyrazolate with electron-withdrawing substituents in the 3 and 5 positions and by using copper(I) or silver(I) as the metal center. Omary et al. reported the synthesis, structures, and photophysical properties of the coinage metal homoleptic series with the ligand 3,5-bis-(trifluoromethyl)pyrazolate.[7] Moreover, the authors concluded that the use of 3,5-bis(trifluoromethyl)pyrazolate as a bridging ligand yields π-acid as well as a metallocycle where the metal center is gold(I); as a matter of fact, the toluene adduct of $[Au(3,5\text{-}(CF_3)_2pz)]_3$ was isolated and structurally characterized. The silver(I) analogue, $[Ag(3,5\text{-}(CF_3)_2pz)]_3$, showed more fascinating properties such as vapochromic selective sensing regarding benzene and its methylated derivatives.[8] The interaction between the metallocycles (A) with arenes or fluoroarenes (B), with the formation of sandwich adducts in the solid state, depends on the electronic and steric features of the metallocycles. The formation of intercalated structures such as the ABAB or BAB type[1,8] is due to the π-acid and π-base electrostatic attractions between the electronic clouds above and below the aromatic and metalloaromatic cycles, as suggested both computationally and experimentally.[6,9] A recent review of such interactions also suggested superior sensing properties of this class of macrometallocyclic d^{10} complexes versus other sensor complexes and materials.[10] However, we note that *removal* of toxic vapor is yet uninvestigated for such small molecular complexes, while this aspect has only been investigated for porous solids such as zeolites, activated carbon, and metal−organic frameworks.[11] The nature of the interaction between the toxic molecule to be removed, on the one hand, and the "filter" material, on the other hand, is desired to be an irreversible process such as chemisorption or decomposition (as opposed to physisorption or weak π-stacking interactions, for example) so as to warrant safe removal of the harmful species. Ammonia vapor, in particular, is highly toxic and regulated by health agencies worldwide. For example, inhalation of ammonia is categorized as "VERY TOXIC, can cause death" by the Canadian Centre for Occupational Health & Safety,[12] while the United States' Centers for Disease Control and Prevention has set an "Immediately Dangerous To Life or Health Concentration" limit of 300 ppm; even more strict short-term exposure limits as little as 25 ppm have been set.[13]

This work is in the context of an ongoing study that we have undertaken to synthesize new pyrazolate and imidazolate coinage metallocycles with π-acid or π-base properties to obtain new materials with potential applications in molecular recognition,[14] sensing,[15] and self-assembled supramolecular architectures possessing optoelectronic properties.[16] These supramolecular structures mainly characterized in the solid state through single-crystal X-ray diffraction have been found to persist even in solution, in a manner akin to what we established earlier for the interaction of π-basic gold(I) trimers with a π-acidic mercury(II) trimer.[17] As a consequence, their formation could not be due to only lattice packing energies. As a prosecution of this study, we now report the synthesis and characterization of a new cyclic trinuclear silver derivative, where the bridging ligand is 3,5-dinitropyrazolate (**1**; see Chart 1). The substitution of trifluoromethyl with nitro groups in the pyrazole ring enhances the electrophile character of the bridging ligand, and in addition to the stacking with naphthalene already observed in the analogous trifluoromethyl-substituted silver derivative,[18] **2**, chemical adsorption properties have been observed for compound **1** with volatile small inorganic and organic molecules. Such molecules containing O, N, or S as donor atoms become chemically adsorbed to **1** after exposure to their vapors. The adducts have been characterized in the solid state by X-ray crystal structure and surface area investigations and in solution by conventional and diffusion ^{1}H NMR techniques.

Chart 1. Trinuclear Cyclic Silver(I) Derivatives Investigated in This Work

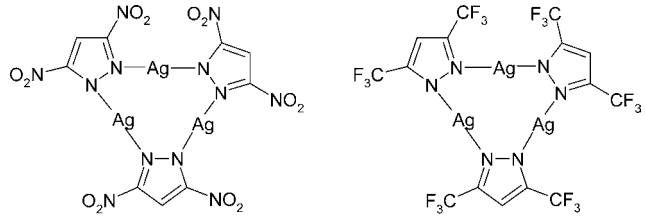

1 **2**

EXPERIMENTAL PART

Synthesis and Characterization. Elemental analyses (C, H, N, and S) were performed in-house with a Fisons Instrument 1108 CHNS-O elemental analyzer. Melting points were taken on an SMP3 Stuart Scientific Instrument. IR spectra were recorded from 4000 to 600 cm^{-1} with a Perkin-Elmer SPECTRUM ONE System FT-IR instrument. IR annotations used: br = broad, m = medium, mbr = medium broad, s = strong, sh = shoulder, w = weak. ^{1}H NMR spectra were recorded on an Oxford-400 Varian spectrometer. Chemical shifts, in ppm, for ^{1}H NMR spectra are relative to internal Me_4Si. NMR annotations used: br = broad, d = doublet, m = multiplet, s = singlet. Electrospray ionization mass spectrometry (ESI-MS) spectra were obtained in positive- or negative-ion mode on a 1100 series MSD detector HP spectrometer, using an acetonitrile mobile phase. The compounds were added to reagent-grade acetonitrile to give solutions with approximate concentrations of 0.1 mM. These solutions were injected (1 μL) into the spectrometer via a HP 1090 series II high-performance liquid chromatography (HPLC) instrument fitted with an autosampler. The pump delivered the solutions to the mass spectrometer source at a flow rate of 300 μL min^{-1}, and nitrogen was employed as both a drying and nebulizing gas. Capillary voltages were typically 4000 and 3500 V for the positive- and negative-ion modes, respectively. Confirmation of all major species in this ESI-MS study was aided by a comparison of the observed and predicted isotope distribution patterns, with the latter calculated using the *IsoPro 3.0* program. The solvents used were HPLC-grade, and they were used as purchased, unless water- and oxygen-sensitive reactions were led. In this last case, anhydrous and free-radical tetrahydrofuran (THF) was obtained by treating the solvent with sodium/acetophenone under a N_2 atmosphere.

Materials. 3,5-Bis(trifluoromethyl)pyrazole and other chemicals were purchased and used without further purification. $AgBF_4$ was purchased by Aldrich and used without any supplementary purification. The synthesis of the 3,5-dinitropyrazolate ligand was led as previously reported in the literature;[19] only the purification was led with a slight modification to obtain the pure sodium salt. In fact, after the second pyrolysis, the mixture of 3,5-dinitropyrazole and 3-nitropyrazole was treated with 1 M NaOH. The resulting salts were then acidified by glacial CH_3COOH until pH 5 to protonate only 3-nitropyrazole. The pure sodium 3,5-dinitropyrazolate was extracted with hot benzene and obtained as a solid with a yield of more than

dx.doi.org/10.1021/ic401948p | *Inorg. Chem.* 2013, 52, 14124−14137

70%. Compound **2** was obtained according to the procedure published by Dias et al.[20]

X-ray Crystal Structure Determination. Crystal structure determination for compounds **1**·2CH_3CN and **3** was carried out using a Bruker SMART APEX2 CCD-based X-ray diffractometer equipped with a low-temperature device and Mo-target X-ray tube (wavelength = 0.71073 Å). Measurements were taken at 100(2) K. Data collection, indexing, and initial cell refinements were carried out using *APEX2*,[21] while frame integration and final cell refinements were done using *SAINT*.[22] An absorption correction was applied using the program *SADABS*.[23] All non-H atoms were refined anisotropically. The H atoms in the compounds were placed in idealized positions and refined as riding atoms. Structure solution, refinement, graphics, and generation of publication materials were performed using *SHELXTL* software.[24] Refinement details and structural parameters for the investigated compounds **1**·2CH_3CN and **3** are summarized in Table 3.

Studies of Adsorption of Volatile Compounds. Adsorption of the vapors on compounds **1** and **2** was led by an in-house procedure. A microcrystalline sample of **1** or **2** was put in a watch glass and allowed to adsorb vapors inside a glass bell saturated with the chosen vapor. The vapor pressure inside the bell was ensured by the spontaneous evaporation of the liquid at room temperature (25 °C). The solvents involved in this procedure of adsorption were used as purchased without any further purification. The adsorptions were monitored by IR spectroscopy, and the adsorption analyses were performed by comparing the spectrum of the adsorbed molecule of both the pure liquid and the "naked" compound **1**. The increase of the intensity of characteristic bands versus time was observed. Adsorption was prolonged until the intensity of the bands stopped changing over time. Then the adducts were put in a vacuum pump for 2 h at 25 °C. The samples then obtained were characterized. Following this method, adsorption with the same volatile compounds were attempted on compound **2**, but it did not adsorb any vapors. The desorption was completely achieved for acetone (Ac) or acetylacetone (AcAc) adducts by washing with THF. After drying in the vacuum, the starting "naked" silver compound was obtained. Readsorption can occur after the washing−drying treatment.

Thermogravimetric Analyses (TGA). TGA was carried out by a thermoanalyzer (TG-DTA; Netzsch STA 490) at a heating rate of 10 °C min^{-1} with 30 mL min^{-1} of air flow.

N_2 Adsorption−Desorption Isotherms. The N_2 adsorption−desorption isotherms were determined by N_2 adsorption at −196 °C using a Micromeritics ASAP 2010 apparatus. Before analysis, the samples were degassed at room temperature overnight. The specific surface area was determined by the Brunauer−Emmett−Teller (BET) method, while the porosity was evaluated by BJH and *t*-plot analysis.[25]

Diffusion NMR Measurements. Diffusion NMR measurements were performed using the standard pulsed-field gradient spin-echo (PGSE) stimulated echo sequence on a Bruker AVANCE DRX 400 spectrometer equipped with a GREAT 1/10 gradient unit and a QNP probe with a Z-gradient coil, at 297 K without spinning. The dependence of the resonance intensity (I) on a constant waiting time and on a varied gradient strength (G) is described by the following equation:

$$\ln \frac{I}{I_0} = -(\gamma\delta)^2 D_t\left(\Delta - \frac{\delta}{3}\right)G^2$$

where I = intensity of the observed spin echo, I_0= intensity of the spin echo in the absence of a gradient, Δ = delay between the midpoints of the gradients, δ = length of the gradient pulse, and γ = magnetogyric ratio. The shape of the gradient was rectangular, their duration (δ) was 4−5 ms, and their strength (G) was varied during the experiments. All of the spectra were acquired using 32K points and a spectral width of 5000 and processed with a line broadening of 1.0 (1H). The semilogarithmic plots of $\ln(I/I_0)$ versus G^2 were fitted using a standard linear regression algorithm, and an R factor higher than 0.99 was always obtained.

Different values of Δ, as well as a number of transients and a number of different gradient strengths (G), were used for different samples. The self-diffusion coefficient D_t, which is directly proportional to the slope of the regression line (m) obtained by plotting $\ln(I/I_0)$ versus G^2, was estimated by measuring the proportionality constant using a sample of HDO (5%) in D_2O (known diffusion coefficients in the range 274−318 K) in the same exact conditions as the sample of interest using the solvent THF as the internal standard. D_t data were treated as described in the literature. The measurement uncertainty was estimated by determining the standard deviation of m by performing experiments with different Δ values. Standard propagation of error analysis yielded a standard deviation of approximately 3−4% in the hydrodynamic radius. D_t* values were obtained by correcting the measured D_t for the viscosity of the solution considering the ratio between m values of the pure solvent and the solvent in the investigated solution.

NMR samples were prepared by dissolving a suitable amount of complexes in approximately 0.6 mL of THF-d_8 to have clear solutions without any precipitate and kept at least 30 min before the measurements were performed. THF-d_8 was purchased from Cortecnet and used as received.

Computational Methodology. All geometry optimizations of $[Ag((NO_2)_2pz)]_3$, $[Ag((CF_3)_2pz)]_3$, and $\{[Ag((CF_3)_2pz)]_3\}_2$ were performed using the *Gaussian 09* suite of programs.[26] The B3LYP hybrid[27] and M06 meta-hybrid[28] functionals were utilized in conjunction with the CEP-31G(d) basis set where d signifies the addition of a d-polarization function to main-group elements.[29−31] Although other methods exist, we adopted M06 as recommended by Zhao and Truhlar to be most suitable as a universal density functional in the study of systems with predominantly noncovalent interactions.[28]

Syntheses. *Synthesis of 1.* To a solution of sodium 3,5-dinitropyrazolate (0.540 g, 3.0 mmol) in 15 mL of THF was added solid $AgBF_4$ (0.582 g, 3.0 mmol). The ready precipitation of a solid was observed. The pale-yellow suspension was stirred for 2 h at room temperature, and then the white solid was removed by filtration. The solid was washed with water and dried (0.215 g), while the THF solution was evaporated to dryness, obtaining a pale-yellow solid. The latter was washed with CH_3OH (3 × 5 mL) and dried (0.235 g). The solid precipitated, and the solid obtained by drying of the THF solution gave the same analytical and spectroscopic characterization, giving 0.460 g of the analytical sample **1**. Yield: 60%. Mp: 245 °C (dec). ^{1}H NMR (acetone-d_6, 293 K): δ 7.80 (s, 3H, C−H pz). ^{1}H NMR (THF-d_8, 293 K): δ 7.91 (s, 3H, C−H pz). IR (cm^{-1}): 3140m (C-Hpz), 1689w, 1550s, 1534ssh, 1490,vs, 1458s, 1359s, 1328vs, 1194m, 1125m, 1078m, 1046m, 1011m, 834vs, 816ssh, 747vs. ESI-MS (major negative ions, CH_3CN): m/z 157 (100) "$[3,5\text{-}(NO_2)_2pz]^-$, 421 (40) $[Ag(3,5\text{-}(NO_2)_2pz)_2]^-$, 950 (30) $[Ag_3(3,5\text{-}(NO_2)_2pz)_4]^-$. Anal. Calcd for $C_9H_3Ag_3N_{12}O_{12}$: C, 13.60; H, 0.38; N, 21.15. Found: C, 13.75; H, 0.31; N, 20.29.

Compound 1·Ac. A total of 30 mg of complex **1** were exposed to acetone vapors in a holder containing acetone at room temperature and atmospheric pressure. Crystals of **1**·Ac were obtained in the following way: 30 mg of complex **1** was dissolved in 3:1 acetone/THF and crystals were obtained by leaving the solution to hexane vapors. Mp: 270 °C (dec). ^{1}H NMR (THF-d_8, 293 K): δ 7.91 (s, 3H, C−H pz), 2.02 (s, 6H, $-CH_3$). IR (cm^{-1}): 3151w (C-Hpz), 1671s (C═O, acetone), 1548s, 1489vs, 1458s, 1358vs, 1327vs, 1234.8m, 1190m, 1074m, 1044s, 1011m, 832vs, 742vs. Anal. Calcd for $C_{12}H_9Ag_3N_{12}O_{13}$: C, 16.90; H, 1.06; N, 19.71. Found: C, 16.68; H, 0.90; N, 19.16.

Compound 1·AcAc. A total of 30 mg of complex **1** was exposed to acetylacetone vapors in a holder containing acetylacetone at room temperature and atmospheric pressure. Mp: 260 °C (dec). ^{1}H NMR (THF-d^8, 293 K): δ 7.91 (s, 3H, C−H pz), 3.55 (s, 2H, $-CH_2$), 2.11 (s, 4H), 1.98 (s, 2H). IR (cm^{-1}): 3142m (C−H pz), 1714m (C═O), 1664s (C═O), 1550s, 1489vs, 1460s, 1360s, 1324vs, 1230m, 1191m, 1165m, sh, 1085m, 1076m, 1047s, 1011m, 833vs, 813ssh, 749s, 741vs. ESI-MS (major positive ions, CH_3CN): m/z 188.9 (100) $[Ag(CH_3CN)_2]^+$. ESI-MS (major negative ions, CH_3CN): m/z 157 (10) $[3,5\text{-}(NO_2)_2pz].^-$, 421 (100) $[Ag(3,5\text{-}(NO_2)_2pz)_2]^-$, 950 (80) $[Ag_3(3,5\text{-}(NO_2)_2pz)_4]^-$, 1216 (30) $[Ag_4(3,5\text{-}(NO_2)_2pz)_5]^-$, 1479 (50) $[Ag_5(3,5\text{-}(NO_2)_2pz)_6]^-$. Anal. Calcd for $C_{14}H_{11}Ag_3N_{12}O_{14}$: C, 18.79; H, 1.24; N, 18.78. Found: C, 19.07; H, 1.17; N, 18.39.

Compound 1·2CH$_3$CN. A total of 30 mg of complex **1** was exposed to acetonitrile vapors in a holder containing acetonitrile at room temperature and atmospheric pressure. Crystals of **1**·2CH$_3$CN suitable for X-ray crystal structure determination were obtained in the following way: 30 mg of complex **1** was dissolved in hot acetonitrile, and then the solution was exposed to diethyl ether vapors. After a few hours, pale-yellow crystals grew from the solution. Mp: 280 °C (dec). ^{1}H NMR (THF-d_8, 293 K): δ 7.91 (s, 3H, C−H pz), 1.95 (s, 6H, CH$_3$CN). IR (cm^{-1}): 3147m (C-Hpz), 2256m (CN, CH$_3$CN), 1655w, 1536s, 1523ssh, 1485vs, 1450s, 1363s, 1357s, 1327vs, 1206m, 1186m, 1076m, 1038m, 1011m, 930w, 826vs, 747vs. Anal. Calcd for $C_{11}H_9Ag_3N_{14}O_{12}$: C, 17.81; H, 1.03; N, 22.36. Found: C, 17.84; H, 0.94; N, 21.70.

Compound 1·3NH$_3$. A total of 30 mg of complex **1** was exposed to NH$_3$ vapors obtained by the solution of 30% (w/w) NH$_4$OH at room temperature and atmospheric pressure. Mp: 230 °C (dec). ^{1}H NMR (THF-d_8, 293 K): δ 7.52 (s, 3H, C−H pz), 2.97 (s, br, 9H, NH$_3$). IR (cm^{-1}): 3389.2m (ν_a NH$_3$), 3307.5 (ν_s NH$_3$), 3155.3 (C-Hpz), 1601w (δ_d NH$_3$), 1538s, 1475vs, 1446s, 1347vs, 1314vs, 1282m, 1176m, 1155m (δ_s NH$_3$), 1075m, 1023m, 999m, 829.8vs, 747vs. ESI-MS (major positive ions, CH$_3$CN): *m*/*z* 188.9 (100) [Ag(CH$_3$CN)$_2$]$^+$. ESI-MS (major negative ions, CH$_3$CN): *m*/*z* 157 (20) [3,5-(NO$_2$)$_2$Pz]$^-$, 421 (100) [(3,5-(NO$_2$)$_2$Pz)$_2$Ag]$^-$, 950 (60) [(Ag(3,5-NO$_2$Pz))$_3$ + (3,5-NO$_2$Pz)$^-$], 1216 (20) [(Ag(3,5-NO$_2$Pz)$_4$ + (3,5-NO$_2$Pz)$^-$], 1479 (30) [(Ag(3,5-NO$_2$Pz))$_5$ + (3,5-NO$_2$Pz)$^-$]. Anal. Calcd for $C_9H_{12}Ag_3N_{15}O_{12}$: C, 12.77; H, 1.43; N, 24.84. Found: C, 13.06; H, 1.35; N, 24.10.

[Ag$_3$-μ-(Pz)$_4$][Ag(NH$_3$)$_2$] (3). By dissolution of 0.050 g of a microcrystalline powder of compound **1**·3NH$_3$ in hot THF (5 mL), a pale-yellow solution was obtained. After filtering through paper, the solution was exposed to diethyl ether vapors and 0.040 g of pale-yellow crystals was obtained after 1 day. Yield: 93%. Mp: 170 °C (dec). ^{1}H NMR (THF-d_8, 293 K): δ 7.66 (s, 4H, C−H pz), 3.022 (s, br, 6H, NH$_3$). IR (cm^{-1}): 3649m, 3384 (ν_aNH$_3$), 3295 (ν_s NH$_3$), 3156 (C-Hpz), 1607w (δ_dNH$_3$), 1533s (NO$_2$), 1476vs, 1455s, 1362vs, 1328vs, 1297m, 1186m, 1070m (δ_s NH$_3$), 1041m, 1033m, 1024m, 1006m, 834vs, 815m, 808m, 740s. ESI-MS (major positive ions, CH$_3$CN): 188.9 (100) [Ag(CH$_3$CN)$_2$]$^+$. ESI-MS (major negative ions, CH$_3$CN): *m*/*z* 157 (70) [3,5-(NO$_2$)$_2$pz]$^-$, 421 (100) [Ag(3,5-(NO$_2$)$_2$pz)$_2$]$^-$, 950 (80) [Ag$_3$(3,5-(NO$_2$)$_2$pz)$_4$]$^-$, 1216 (20) [Ag$_4$(3,5-(NO$_2$)$_2$pz)$_5$]$^-$, 1479 (50) [Ag$_5$(3,5-(NO$_2$)$_2$pz)$_6$]$^-$. Anal. Calcd for $C_9H_{12}Ag_3N_{15}O_{12}$: C, 13.18; H, 0.92; N, 23.05. Found: C, 13.37; H, 0.85; N, 22.64.

Compound 1·3py. A total of 30 mg of complex **1** was exposed to pyridine vapors by putting the solid sample in a holder containing anhydrous pyridine at room temperature and atmospheric pressure. Mp: 204.2−206.0 °C (dec). ^{1}H NMR (THF-d_8, 293 K): δ 8.59 (m, 6H, CH−N), 7.78 (m, 3H, *p*-CH), 7.73 (s, 3H, C−H pz), 7.39−7.36 (m, 6H, *m*-CH). IR (cm^{-1}): 3152m (C−H pz), 3103w (C−H py), 3038w (C−H py), 1655w (C═C py) 1598m (C═N py), 1541vs, 1524m, 1481vs, 1446s, 1351vs, 1323vs, 1289m, 1216m, 1179s, 1076m, 1069m, 1030s, 1001m, 883m, 832vs, 815m, 748vs, 699vs, 676m. ESI-MS (major positive ions, CH$_3$CN): 80.2 (100) [py + H]$^+$, 188.9 (50) [Ag(CH$_3$CN)$_2$]$^+$. ESI-MS (major negative ions, CH$_3$CN): *m*/*z* 157 (100) [3,5-(NO$_2$)$_2$pz]$^-$. Anal. Calcd for $C_{24}H_{18}Ag_3N_{15}O_{12}$: C, 27.93; H, 1.76; N, 20.36. Found: C, 28.36; H, 1.66; N, 19.59.

Compound 1·$^1/_2$Et$_3$N. A total of 30 mg of complex **1** was exposed to Et$_3$N vapors by putting the solid sample in a holder containing Et$_3$N at room temperature and atmospheric pressure. Mp: 116 °C (dec). ^{1}H NMR (THF-d_8, 293 K): δ 7.84 (s, 3H, C−H pz), 2.75 (q, 6H, NCH$_2$), 1.20 (t, 9H, −CH$_3$). IR (cm^{-1}): 3136m (C−H pz), 2967w, 2925w, 2849w, 1544s, 1484vs, 1457m, 1357s, 1326vs, 1200m, 1178m, 1078m, 1047m, 1027m, 1011m, 1001m, 833s, 741vs, ESI-MS (major positive ions, CH$_3$CN): *m*/*z* 102.2 (100) [Et$_3$N + H]$^+$. ESI-MS (major negative ions, CH$_3$CN): *m*/*z* 157 (20) [3,5-(NO$_2$)$_2$pz]$^-$, 421 (100) [Ag(3,5-(NO$_2$)$_2$pz)$_2$]$^-$, 950 (60) [Ag$_3$(3,5-(NO$_2$)$_2$pz)$_4$]$^-$, 1216 (20) [Ag$_4$(3,5-(NO$_2$)$_2$pz)$_5$]$^-$, 1479 (30) [Ag$_5$(3,5-(NO$_2$)$_2$pz)$_6$]$^-$. Anal. Calcd for $C_{24}H_{21}Ag_6N_{25}O_{24}$: C, 17.59; H, 1.23; N, 19.97. Found: C, 17.05; H, 1.25; N, 20.71.

Compound 1·3THT. A total of 30 mg of complex **1** was exposed to tetrahydrothiophene (THT) vapors by putting the solid sample in a holder containing THT at room temperature and atmospheric pressure. Mp: 178.8−180.3 °C. ^{1}H NMR (THF-d_8, 293 K): δ 7.72 (s, 3H, C−H pz), 2.97 (t, 12H, S−CH$_2$), 2.02 (m, 12H, −CH$_2$). IR (cm^{-1}): 3155m (C−H pz), 2950m, 2923w, 2852w, 1540s, 1526ssh, 1482vs, 1449m, 1356s, 1327vs, 1289m, 1250m, 1175m, 1130w, 1068m, 1029m, 1005m, 954m, 881m, 834s, 815m, 745s. ESI-MS (major positive ions, CH$_3$CN): 188.9 (100) [Ag(CH$_3$CN)$_2$]$^+$. ESI-MS (major negative ions, CH$_3$CN): *m*/*z* 157 (100) [3,5-(NO$_2$)$_2$pz]$^-$. Anal. Calcd for $C_{21}H_{27}Ag_3N_{12}O_{12}S_3$: C, 23.81; H, 2.57; N, 15.87; S, 9.08. Found: C, 23.94; H, 2.45; N, 15.59; S, 8.85.

Compound 1·2Me$_2$S. A total of 30 mg of complex **1** was exposed to Me$_2$S vapors by putting the solid sample in a holder containing THT at room temperature and atmospheric pressure. The adduct is not soluble in most common solvents. Mp: 250 °C (dec). IR (cm^{-1}): 3157m (C−H pz), 2931w, 1557s, 1531s, 1487vs, 1450m, 1354sh, 1324vs, 1204m, 1077m, 1036m, 1001m, 830s, 743s. Anal. Calcd for $C_{13}H_{15}Ag_3N_{12}O_{12}S_2$: C, 16.99; H, 1.65; N, 18.29; S, 6.98. Found: C, 16.28; H, 1.13; N, 17.83; S, 6.54.

RESULTS AND DISCUSSION

Syntheses and Spectroscopic Characterizations. The trinuclear silver derivatives **1** and **2** were obtained in good yield by following the procedures published by Fackler et al.[32] and by Dias et al.,[20] respectively. The synthesis of stable trinuclear cyclic derivatives with 3,5-dinitropyrazolate was not successful when gold(I) and copper(I) precursors were used. In fact, the reaction of Ph$_3$PAuCl or Ph$_3$AsAuCl with sodium 3,5-dinitropyrazolate yielded the mononuclear derivative, (3,5-dinitro-1*H*-pyrazolat-1-yl)triphenylphosphinegold(I), in high yield, which being soluble in polar and protic solvents was successfully tested as an anticancer drug.[33] Compound **1** is a pale-yellow solid, stable both in solution and in the solid state. Crystals of **1** as the solvent adduct were obtained from acetone by adding hexane or from acetonitrile solutions. From THF, diethyl ether, or alcoholic solutions, the "naked" (unsolvated) compound **1** was isolated as a microcrystalline solid. This latter sample was employed in the adsorption studies as a reference compound. Resolutions of all crystal structure attempts by X-ray diffraction have shown the presence of solvent molecules in the unit cell of **1**. These results prompted us to thoroughly investigate the interaction of volatile compounds with compounds **1** and **2**. Surprisingly, the adsorptions occurred even under mild conditions of pressure and temperature, and only for compound **1**. In particular, when a solid sample of compound **1** was exposed to vapors of acetone, acetylacetone, acetonitrile, ammonia, pyridine, triethylamine, tetrahydrothiophene, or dimethyl sulfide, the respective adducts were obtained in a few minutes, giving rise to **1**·Ac, **1**·AcAc, **1**·2CH$_3$CN, **1**·3NH$_3$, **1**·3py, **1**·$^1/_2$Et$_3$N, **1**·3THT, and **1**·2Me$_2$S. The adducts were analyzed and characterized, showing a molar ratio between compound **1** and the adsorbed molecules depending on the identity of the adsorbed molecule. Adsorption experiments were attempted also with carbon monoxide (CO), THF, methanol, ethanol, and diethyl ether without success. To analyze the electrophilic nature of **1**, a comparative study with another π-acid silver metallocyclic complex **2** has also been performed. Studies on the analogous compound **2** were carried out under the same experimental conditions, and no adsorption was detected in all cases. Moreover, to test the electrophilic nature of **1**, the reaction between **1** and naphthalene was carried out to obtain an insoluble white solid, which spectroscopic characterization reveals as the likely stacked structure analogous to that obtained

dx.doi.org/10.1021/ic401948p | *Inorg. Chem.* 2013, 52, 14124−14137

with **2**[18] (see the Supporting Information, SI). An attempt to crystallize compound **1**·3NH_3 yielded compound **3**. Elemental analysis revealed that the latter corresponds to four Ag atoms bonded to four pyrazolate ligands and two molecules of ammonia. The resolution of the crystal structure has shown that the starting metallocyclic silver unit has rearranged in the solution. The final structure preserves a trinuclear silver cycle, but two silver ions are supported by a further bridging pyrazolate, whereas the two ammonia molecules are actually coordinated to a silver ion, forming the cationic complex $[Ag(NH_3)_2]^+$. Given the extremely high formation constant (1.6×10^7 at 25 °C),[34] this ultimate rearrangement of ammonia from the vapor phase to its containment in a solid salt is highly desirable for toxic gas filtration applications.

The characterization of all adducts and compounds **1** and **3** has been performed in the solid state by elemental analysis, IR spectroscopy, and when possible in solution by ESI-MS and in THF-d_8 solutions by ^{1}H NMR spectroscopy. X-ray crystal structure determinations were carried out for **1**·2CH_3CN and compound **3** (see below). ^{1}H NMR characterizations show mild shifts that are diagnostic of interactions also in solution. For example, the C_4−H pyrazole ^{1}H NMR signals of the acetone (**1**·Ac), acetylacetone (**1**·AcAc), and acetonitrile (**1**·2CH_3CN) adducts compared well with those of the starting compound **1** without any significant shifts in resonances, while such shifts become significant in the case of the ammonia (**1**·3NH_3), pyridine (**1**·3py), triethylamine (**1**·$^1/_2Et_3N$), and tetrahydrothiophene (**1**·3THT) adducts and of compound **3**. On the side of the adsorbed molecule, taking as an example the pyridine adduct **1**·3py, the three patterns due to the aromatic ring recorded in THF-d_8 (py) undergo low-frequency mild shifts such as from 8.55 (py) to 8.60 (**1**·3py), from 7.66 (py) to 7.79 (**1**·3py), and from 7.28 (py) to 7.37 (**1**·3py), suggesting weak interactions in solution. The variations on the chemical shift could be attributed to interaction between the pyrazolate and adsorbed molecules; however, detailed PGSE NMR studies indicate that only the THT adduct persists in THF in a significant amount. The solution characterization was also performed with ESI-MS. The adducts were not detected as molecular peaks. As an overall behavior, cleavage and rearrangement of the metallocycles were detected with the formation of $[Ag(CH_3CN)_2]^+$ and $[3,5\text{-}pz(NO_2)_2]^-$ as common ions in acetonitrile solutions. In the case of the **1**·3py and **1**·$^1/_2Et_3N$ adducts, the protonated pyridine and triethylamine species were found in the positive field. Small amounts of higher-nuclearity species were recorded in some adduct spectra, giving patterns due to $[Ag_4(3,5\text{-}(NO_2)_2pz)_5]^-$ and $[Ag_5(3,5\text{-}(NO_2)_2pz)_6]^-$ ions. This behavior was observed in most of the adducts but not in the mass spectrum of the starting compound **1**. The IR spectra are more diagnostic of adsorption either because they were recorded in the solid state and for a better sensitivity of the technique. The C_4−H pyrazole stretching vibrations range from 3140 cm^{-1} for **1** and 3147 cm^{-1} for **1**·2CH_3CN to 3155 cm^{-1} for **1**·3THT, and similar shifts were observed for the other typical bands of the pyrazole ligand. On the side of the adsorbed molecules, larger shifts ranging between 5 and 40 cm^{-1} are evidenced. The case of the **1**·AcAc adduct is interesting. In fact, in the free acetylacetone, three diagnostic bands are recorded in the region below 1800 cm^{-1} because of the combination of the carbonyl stretching, the C═C stretching, and the bending of the OH of the tautomeric forms (1728, 1708, and 1605 cm^{-1});[35] in the adduct, in contrast, only two bands are recorded at 1714 and 1664 cm^{-1}. In the pyridine adduct **1**·3py, the typical bands of the C−H and C═C pyridine stretching vibrations were found with appreciable blue shifts vs free pyridine. Crystallization of the ammonia adduct **1**·3NH_3 yielded compound **3**. The early spectroscopic characterizations showed markedly different spectra in both ^{1}H NMR and IR. The ammonia adduct ^{1}H NMR spectrum shows a signal for the C_4−H pyrazole at 7.52 ppm, which shifts to 7.66 ppm in compound **3**. The NH_3 broad signal falls at 2.97 ppm for the adduct with an integral proper for a 1:3 molar ratio of complex **1**/ammonia; in compound **3**, this signal was recorded at 3.02 ppm with an integral proper for four pyrazole ligands and two NH_3 molecules. In the high-energy region of the IR spectra, these differences are more evident in the adduct for which the asymmetric and symmetric stretching bands of the N−H bonds were observed at 3389 and 3307 cm^{-1}, respectively, compared to 3384 and 3295 cm^{-1}, respectively, in compound **3**. The bending deformation was also shifted because it was observed at 1601 cm^{-1} for the adduct and at 1607 cm^{-1} for compound **3**. An additional band in the high-energy region was observed at 3649 cm^{-1} for **3**, which can be attributed to the hydrogen bonding occurring between the H atoms of NH_3 and the O atoms of the nitro groups, as confirmed in the X-ray crystal structural data. The single-crystal X-ray diffraction showed a structure where the ammonia is not coordinated to the metallocycle, and it forms the $[Ag(NH_3)_2]^+$ cation as discussed in the following section.

Crystal Structures. Compound **1**·2CH_3CN crystallizes in the monoclinic crystal system (*C*2/*c* space group). The molecular structure is shown in Figure 1, whereas the main

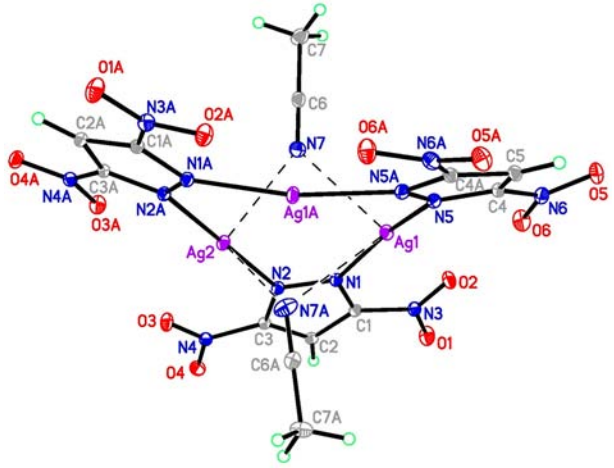

Figure 1. General view of **1**·2CH_3CN with two CH_3CN solvent molecules interacting with the Ag atoms.

bond lengths, valence, and dihedral angles are listed in Table 1. Crystallographic data are reported in Table 3. The nonplanar nine-membered cycle is formed by three centers of silver and three bridging 3,5-dinitropyrazolate ligands. The Ag2−N2 and Ag2−N2A bond lengths are equal to 2.176(1) Å, while for the weakest interacting silver center, the Ag1−N1 and Ag1−N5 bond lengths are 2.184(1) and 2.182(1) Å, respectively. These distances are similar to those found in similar pyrazolate metallocycles and in compound **2**.[7,20,32,36b,c] The nine-membered cycle is nonplanar with a deviation of the planarity of 0.1793 Å. Two CH_3CN solvent molecules are coordinated to Ag2 (Ag2···N7/N7A) with a distance of 2.590(1) Å. In comparison, the distance Ag1/Ag1A···N7/N7A is 2.647(1) Å.

dx.doi.org/10.1021/ic401948p | *Inorg. Chem.* 2013, 52, 14124−14137

Table 1. Bond Distances (Å) and Valence and Dihedral Angles (deg) for 1·2CH$_3$CN[a]

Ag1−N5	2.182(1)
Ag1−N1	2.184(1)
Ag2−N2	2.176(1)
Ag2−N7	2.590(1)
Ag1−N7	2.647(1)
N1−N2	1.335(2)
N5−N5A#1	1.347(2)
N5−Ag1−N1	165.36(4)
N2−Ag2−N2A#1	179.96(6)
Ag1−N1−N2−Ag2	8.9(1)
Ag1−N5−N5A−Ag1A#1	−9.5(1)

[a]Symmetry transformations used to generate equivalent atoms: #1, $-x + 1, y, -z + {}^1/_2$.

The value of the bond angle N1−Ag1−N5 is 165.36(4)° and is distinctly smaller than the linear angle N2−Ag2−N2A [179.96(6)°]. Such a strong deviation from linearity has already been observed in an analogous Ag$_3$ derivative, {[3-(CF$_3$)-5-(Bu^t)Pz)Ag]$_3$},[36b,c] where the pyrazolate bridging ligand is not symmetrical with a value of the N−Ag−N angle of 166.9(2)°, and in this case, the deviation was attributed to the steric hindrance of the *tert*-butyl in the 5 position. In **1**·2CH$_3$CN, intramolecular Ag1···Ag2 and Ag1···Ag1A distances are 3.555 and 3.739 Å, respectively. Very weak intermolecular C−H···O hydrogen bonds link trimer and solvent molecules in the crystal, forming a network (Figure 2).

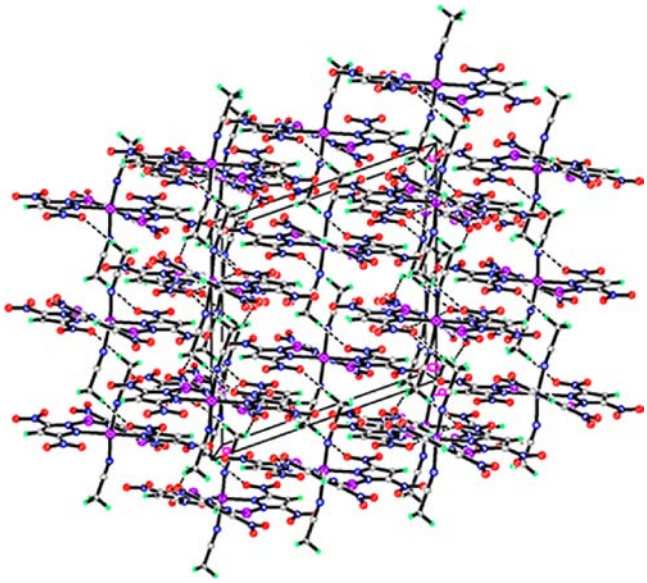

Figure 2. Crystal packing of compound **1**·2CH$_3$CN along the *b* axis. Dashed lines are weak C−H···O hydrogen bonds.

Compound **3** exhibits cocrystallization of $[Ag(NH_3)_2]^+$ with $[Ag_3pz_4]^-$ in the triclinic crystal system ($P\bar{1}$; Figure 3). Bond distances and valence and dihedral angles are reported in Table 2, whereas crystallographic data are listed in Table 3. In the target molecule, there are two different types of Ag atoms: the atoms Ag1 and Ag3 are three-coordinated, while Ag2 is only two-coordinated. Intramolecular Ag1···Ag2, Ag1···Ag3, and Ag2···Ag3 distances are 3.903, 3.613, and 3.797 Å, respectively.

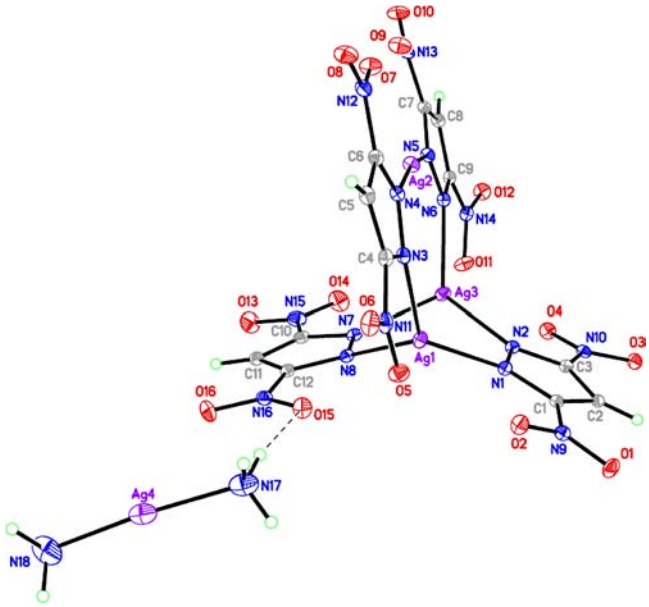

Figure 3. General view of **3** showing the interaction of $[Ag(NH_3)_2]^+$ with the oxygen of the NO$_2$ group belonging to the pyrazole ring.

Table 2. Bond Distances (Å) and Valence and Dihedral Angles (deg) for 3

Ag1−N1	2.218(2)
Ag1−N3	2.237(2)
Ag1−N8	2.301(2)
Ag2−N4	2.133(2)
Ag2−N5	2.126(2)
Ag3−N2	2.237(2)
Ag3−N6	2.230(2)
Ag3−N7	2.280(2)
N1−N2	1.345(3)
N3−N4	1.349(3)
N5−N6	1.347(3)
N7−N8	1.342(3)
N1−Ag1−N3	129.91(7)
N1−Ag1−N8	101.43(7)
N3−Ag1−N8	116.58(7)
N5−Ag2−N4	169.14(7)
N6−Ag3−N2	127.60(7)
N6−Ag3−N7	117.17(7)
N2−Ag3−N7	105.33(7)
Ag1−N1−N2−Ag3	−5.9(2)
Ag1−N3−N4−Ag2	−6.7(2)
Ag2−N5−N6−Ag3	11.0(2)
Ag3−N7−N8−Ag1	8.1(2)

The Ag2 atom forms relatively short intermolecular contact Ag2···Ag2A (3.440 Å) linking two molecules with the formation of a dimer (Figure 4). In the crystal of the complex **3**, relatively strong hydrogen bonds link the target molecule with $[Ag(NH_3)_2]^+$, resulting in a three-dimensional ionic framework (Figure 5 and Table 4).

Adsorption. *Solid-State Characterization.* As discussed in the Introduction, trinuclear silver(I) or gold(I) complexes have been extensively studied for their properties with regards to solvatochromic or vapochromic sensing.[7] Compound **1** shows

dx.doi.org/10.1021/ic401948p | *Inorg. Chem.* 2013, 52, 14124−14137

Table 3. Crystallographic Data for Compounds 1·2 CH_3CN and 3, Respectively

	1·2CH_3CN	3
empirical formula	C_{13} H_9 Ag_3 N_{14} O_{12}	$C_{12}H_4Ag_3N_{16}O_{16}$, AgN_2H_6
fw	876.95	1093.86
temperature, K	100(2)	100(2)
cryst syst	monoclinic	triclinic
space group, *Z*	*C*2/*c*, 4	$P\bar{1}$, 2
a, Å	14.4883(3)	8.5731(3)
b, Å	12.4162(3)	12.2440(5)
c, Å	14.3661(3)	13.8489(5)
α, deg	90	90.032(1)
β, deg	109.604(1)	91.937(1)
γ, deg	90	98.991(2)
volume, $Å^3$	2434.5(1)	1435.0(1)
density, g cm^{-3}	2.393	2.532
final R1	0.0127	0.0199
final wR2	0.0399	0.0455
GOF	1.011	1.025
$\Delta\rho$(max), $\Delta\rho$(min), e $Å^{-3}$	0.405, −0.218	0.590, −0.671

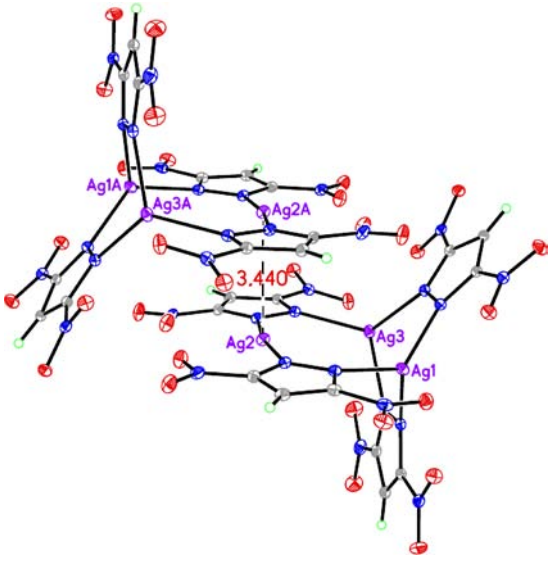

Figure 4. Mutual orientation of two molecules of **3** forming a dimer. The dashed line is a Ag2···Ag2A intermolecular contact.

structural similarities but atypical features compared with other similar silver complexes. Both compounds **1** and **2** possess pyrazole bridging ligands but different withdrawing substituents in the 3 and 5 positions. Compound **2** has been extensively studied in solution for its variable luminescence properties depending upon changes in the temperature or solvent.[36] It stacks with benzene, toluene, and naphthalene to yield columnar structures in the solid state.[1] Moreover, its emission maxima depend on the aromatic vapor that it is in contact with.[8] Compound **1** does not exhibit interesting emission properties, but in the solid state, it adsorbs vapors of volatile compounds bearing O, N, and S donor atoms in a fixed stoichiometric ratio.

With the aim of characterizing the external texture of compound **1**, obtained by THF solutions, N_2 adsorption−desorption isotherms at 77 K on this compound were performed by commercially available volumetric equipment. The obtained adsorption−desorption isotherms are shown in

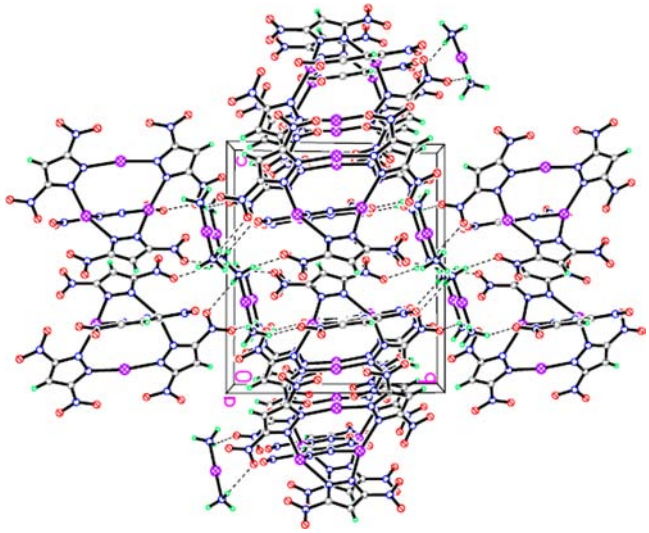

Figure 5. Crystal packing of compound **3** along the *a* axis. Dashed lines are N−H···O hydrogen bonds.

Table 4. Hydrogen Bonds for Compound 3 [Å and deg]

D−H···A[a]	*d*(D−H)	*d*(H···A)	*d*(D···A)	∠DHA
N17−H17B···O15#1	0.91	2.26	3.150(3)	166.0
N17−H17A···O5#2	0.91	2.56	3.361(3)	147.8
N17−H17C···O13#3	0.91	2.52	3.285(3)	142.3
N18−H18A···O6#4	0.91	2.28	3.077(3)	146.4
N18−H18C···O4#5	0.91	2.33	3.059(3)	136.7

[a]Symmetry transformations used to generate equivalent atoms: #1, *x*, *y*, *z*; #2, −*x* + 1, −*y* + 2, −*z* + 1; #3, *x*, *y* + 1, *z*; #4, −*x*, −*y* + 2, −*z* + 1; #5, −*x* + 1, −*y* + 1,−*z* + 1.

Figure 6. The observation of hysteresis between the desorption and adsorption isotherms usually indicates that the solid

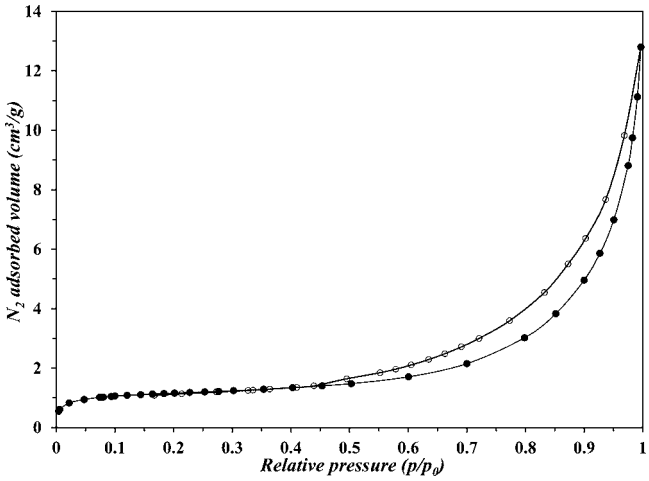

Figure 6. N_2 adsorption−desorption isotherm plot obtained at 77 K for compound **1**. Filled and empty symbols represent adsorption and desorption, respectively.

exhibits mesopores in its structure. However, the calculated mesopore volume is less than 0.02 cm^3 g^{-1} with no evident maximum in the mesopore size distribution curve. Consequently, the sample should be considered nonporous, whereas nonstructural mesopores are likely present between neighboring particles of the solid material. The adsorption

dx.doi.org/10.1021/ic401948p | *Inorg. Chem.* 2013, 52, 14124−14137

isotherm can be classified as type II in the IUPAC classification.[37]

Application of the BET theory[38] to the experimental adsorption data permits us to calculate a specific surface area of 4.15 $m^2\ g^{-1}$ for a powder sample of complex **1**. This low value along with the very low values calculated for micro- and mesopore volumes indicate that adsorption of the vapors is not due to physical adsorption but to chemical interactions with the vapor molecules, which interact with the metallic centers of the trinuclear cycle.

Thermogravimetric Analysis (TGA) and Differential Thermal Analysis (DTA). All of the samples were investigated by TGA and DTA. The thermal behavior of all of the samples involves two weight loss processes for temperatures lower than 500 °C, whereas for temperatures higher than 500 °C, no weight loss was found. The first weight loss can be attributed to an endothermic weight loss due to a loss of adsorbed molecules and the second to an exothermic weight loss due to the full combustion and decomposition of the organic part of the compounds. The TGA profile for the adduct **1**·2CH_3CN is shown in Figure 7.

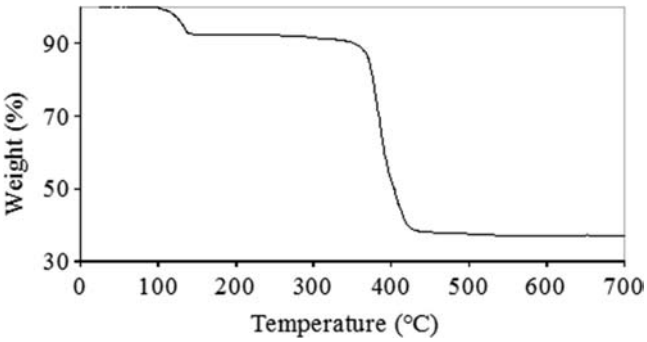

Figure 7. TGA plot for **1**·2CH_3CN.

For all of the samples, the weight loss measured at temperatures higher than 500 °C corresponds to the indicated stoichiometry of the compounds. It is interesting to consider the first endothermic weight loss process: for all of the samples, the percentage mass changes measured are consistent with those calculated for removal of the adsorbed molecules. The temperature range of these processes compared with the boiling point of the pure adsorbed molecules and the experimental and expected weight loss values are summarized in Table 5. The weight loss starts at a higher temperature than the corresponding boiling point; i.e., for the acetone adduct, the weight loss starts at about 80 °C, for the pyridine adduct at 200 °C, for compound **3** at 220 °C, and for the THT adduct at 120 °C. The stepwise loss occurs at temperatures ranging from 200 to 300 °C. These results indicate that, in all adducts, the interactions between molecules adsorbed and the complex are significantly stronger than those occurring in the pure solvents.

In most situations here, thermal removal of the adsorbed molecules occurs in one step, but in the case of the tetrahydrothiophene adduct, **1**·3THT, stepwise loss of the adsorbed molecules has been recorded. Remarkably, the weight loss for the ammonia adduct occurs at up to 200 °C higher than the normal boiling point of −33 °C for NH_3 and rather considerably higher than practical ambient temperatures, which not only underscores the strength of the underlying chemical interaction but also further substantiates the significance of the findings herein toward filtration of toxic chemicals via molecules such as **1**.

Diffusion NMR Studies in Solution. Diffusion NMR measurements[39] were performed for complex **1** and some of its adducts with Lewis bases in THF-d_8 in order to obtain the self-diffusion coefficient (D_t) for both the silver complex and adsorbed species in an independent way, determining the level of association in solution. The D_t value is directly correlated with the hydrodynamic radius through the modified Stokes−Einstein equation:[40]

$$D_t = \frac{kT}{fc\pi\eta r_H}$$

where k is the Boltzmann constant, T is the temperature, η is the fluid viscosity, and r_H is the hydrodynamic radius. f and c are two numerical factors related to the shape of the diffusing molecule and the ratio between the solute and solvent radii, respectively.

As can be easily noted, the shape of complex **1** is far from being considered as spherical and a correct evaluation of the f factor is essential in order to have an accurate estimation of the molecular dimensions in solution. From the X-ray diffraction structure (Figure 8), three limit distances were extrapolated: (i) the maximum molecular radius [i.e., the distance between the molecular centroid and the limit of the van der Waals cloud of

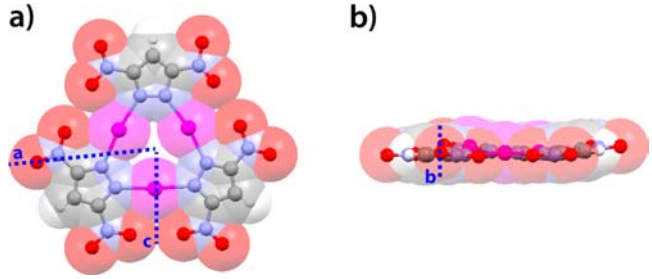

Figure 8. Two different views of the X-ray structure of **1**.

Table 5. Range of Temperatures Weight Loss (°C) and Weight Loss Percentage for the Investigated Adducts (%)

			% weight loss	
compound	range of temperature weight loss (°C)	boiling points (°C, 1 atm)	experimental	expected
1·Ac	100−120	56 (acetone)	5.6	6.8
1·2CH_3CN	100−130	82 (acetonitrile)	8.5	9.4
1·3NH_3	110−170	−33 (ammonia)	6.3	6.0
1·3py	180−220	115 (pyridine)	23.2	23.0
1·$^1/_2$ Et_3N	90−120	90 (triethylamine)	6.0	9.8
1·3THT	120−300	119 (tetrahydrothiophene)	25.2	25.0
3	220−250	−33 (ammonia)	4.1	4.0

dx.doi.org/10.1021/ic401948p | *Inorg. Chem.* 2013, 52, 14124−14137

the farthest O atom of the NO_2 groups (a in Figure 8a, 7.61 Å)]; (ii) the minimum molecular radius [i.e., the distance between the centroid and van der Waals cloud in the middle of the NO_2 groups (c in Figure 8a, 5.17 Å)]; (iii) half of the molecular thickness (b in Figure 8b, 1.38 Å). The molecular shape can be approximated to that of an oblate ellipsoid having the two semiaxes *a* and *b*; the calculated molecular volume is 336 Å^3, while the *f* factor is 1.25.[41]

The results of the PGSE NMR experiments (see the Experimental Part section for details), performed on **1** in THF-d_8, are summarized in Table 6 and show that the measured hydrodynamic volumes fit nicely with that obtained from X-ray diffraction. Because V_H is independent of the concentration, it can be concluded that **1** does not show any tendency to self-aggregate.

Table 6. Diffusion Coefficients (D_t, $\times 10^{-10}$ m^2 s^{-1}), Corrected Diffusion Coefficients (D_t*, $\times 10^{-10}$ m^2 s^{-1}), Hydrodynamic Radii (r_H, Å), and Hydrodynamic Volumes (V_H, Å^3) as a Function of Concentration (*C*, mM) Obtained for 1 in THF-d_8 at 297 K

C	D_t	D_t*	r_H	V_H
0.5	8.28	8.31	4.10	289
1.2	8.22	8.17	4.14	297
3.2	8.19	8.17	4.14	297
7.2	8.04	8.13	4.17	304

As far as the behavior of the adducts is concerned, diffusion NMR studies were performed by dissolving powders of **1**·Ac, **1**·3NH$_3$, **1**·2CH$_3$CN, and **1**·3THT in order to verify whether the **1**·Lewis base adducts persist in solution (Table 7). The most indicative experimental parameter for evaluating the formation of an adduct between the two species is the V_H value of the Lewis base. Indeed, when the latter binds to the larger **1** molecule, an appreciable increase of its V_H should be observed. Therefore, we focused our attention on the V_H values of the adsorbed species. Looking at the whole set of data, it clearly appears that the measured hydrodynamic volumes for acetone, NH_3, and CH_3CN (Table 7) are equal to those of the free molecules[40b] while V_H values of the tripyrazolates are in line with those measured for complex **1**. On the contrary, the V_H value of THT is more than 2 times higher than that expected for a free-diffusing molecule (80 Å^3). This leads to the conclusion that, only in **1**·3THT, the interaction between the organic molecule and the silver tripyrazolate persists in solution (Figure 9). In Figure 10, the ^{1}H NMR spectrum of the complex **1**·3THT is shown and the relative integration of NMR signals indicates the presence of one THT molecule in the vicinity of each Ag atom of the complex. By a comparison of the V_H values for compound **1** and THT, it can be seen that they are not equal. This can be due to the presence of an association equilibrium between the adduct and the free species. However, from the single diffusion measurement, it was not possible to deduce how many molecules of THT interact with silver in solution because of the possible presence of a distribution of species with one or more molecules of THT bound to the Ag atoms.

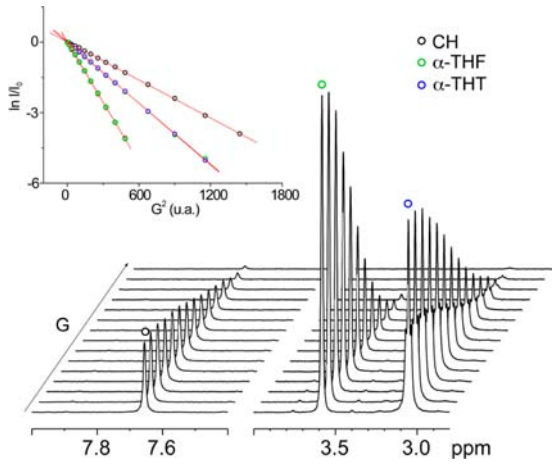

Figure 9. Decay of the NMR signal for the adduct of complex **1** with THT in THF-d_8 (c = 15.8 mM). The linear regression of $\ln(I/I_0)$ versus G^2 is reported in the inset.

Computational Studies. *Chemisorption and Electrostatic Forces.* We start by discussing the CO and acetonitrile interactions with **1** as models representing the two limiting cases for small molecules exhibiting weak versus strong interactions according to the experimental data above. In computation of the adsorption of two CO molecules to $[Ag(3,5\text{-}(NO_2)_2pz)]_3$, **1**, the B3LYP/CEP-31G(d) results

Table 7. Diffusion Coefficients (D_t, $\times 10^{-10}$ m^2 s^{-1}), Corrected Diffusion Coefficients (D_t*, $\times 10^{-10}$ m^2 s^{-1}), Hydrodynamic Radii (r_H, Å), and Hydrodynamic Volumes (V_H, Å^3) as a Function of Concentration (*C*, mM) Obtained for Adducts 1·Ac, 1·3NH$_3$, 1·2CH$_3$CN, and 1·3THT in THF-d_8 at 297 K

	1[a]				adsorbed molecule			
C, mM	D_t	D_t*	r_H	V_H	D_t	D_t*	r_H	V_H
				Ac				
0.9	8.28	8.31	4.10	289	8.28	8.31	4.10	30
2.2	8.22	8.17	4.14	297	8.22	8.17	4.14	30
6.5	8.19	8.17	4.14	297	8.19	8.17	4.14	30
				NH_3[b]				
1.2	11.6	11.8	3.01	114	34.3	34.7	2.07	37
				CH_3CN				
11.3	9.97	9.50	3.74	219	31.4	29.9	2.22	46
				THT				
8.8	7.90	8.13	4.90	493	1.27	1.30	3.52	183
15.3	7.63	8.06	4.94	505	1.13	1.19	3.73	217

[a]Volumes of **1** are treated spherically in the case of the THT adduct. [b]The small value of the hydrodynamic volume can be ascribed to some decomposition of the complex.

dx.doi.org/10.1021/ic401948p | *Inorg. Chem.* 2013, 52, 14124−14137

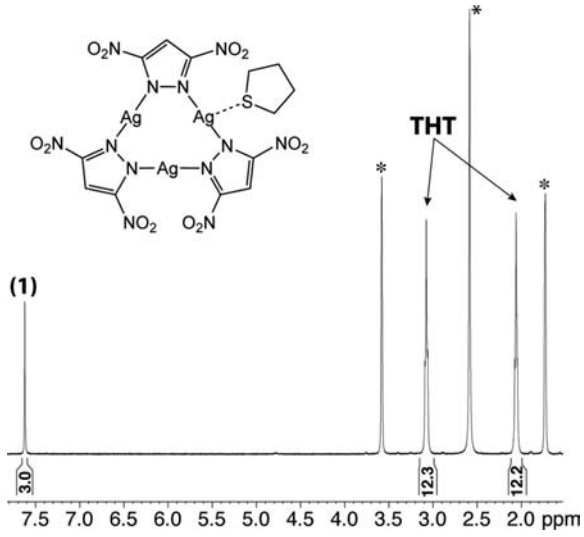

Figure 10. ^{1}H NMR spectrum of the adduct **1**·3THT recorded in THF-d_8 at 297 K (c = 15.2 mM). Asterisks denote residue of protonated D_2O and THF-d_8.

show a vanishingly weak binding energy of 1.4 kcal mol^{-1}. The binding energy for one trimer **1** molecule to one and two CH_3CN molecules was 8.5 and 15.9 kcal mol^{-1}, respectively, according to the same B3LYP/CEP-31G(d) methodology. This result suggests that the addition of a second CH_3CN molecule is additive, i.e., neither cooperative nor inhibitive. Those B3LYP/CEP-31G(d) results are *qualitatively* in agreement with the experimental data in that they explain the experimental formation of a binary adduct with **1** for acetonitrile but not CO. However, the aforementioned binding energies are closer to the physisorption range as opposed to chemisorption. Using the M06 functional, which is known to better model dispersion forces than B3LYP, improves the description of the attractive forces to yield a binding energy of 26.9 kcal mol^{-1} for the **1**·2CH_3CN binary adduct. This energy is high enough to be deemed chemisorption instead of physisorption. Therefore, we conclude that the M06/CEP-31G(d) results for the **1**·2CH_3CN binary adduct are in agreement with the experimental data both *qualitatively* and *quantitatively*, with the latter being manifested by the binding energy representing chemisorption instead of physisorption, consistent with the BET surface area and TGA data above.

Figure 11 illustrates additional insights on the associated nature of attractive forces based on molecular electrostatic potential (MEP) computations. Although the 3-fold rotation in the [Ag(3,5-$(NO_2)_2$pz)]$_3$ model (D_{3h} effective symmetry) precludes dipole, the molecule is strongly quadrupolar with a rather strong π-acidic behavior at the center of the nine-membered macrometallocyclic ring and normal regions thereof in both sides. Therefore, these strongly electron-deficient regions are available to significant quadrupole–dipole interactions with the Lewis-basic acetonitrile molecule. The nonvanishing traceless quadrupole moment tensors (field-independent basis) are −17.4, −17.4, and 35.2 D Å representing Q_{xx}, Q_{yy}, and Q_{zz},

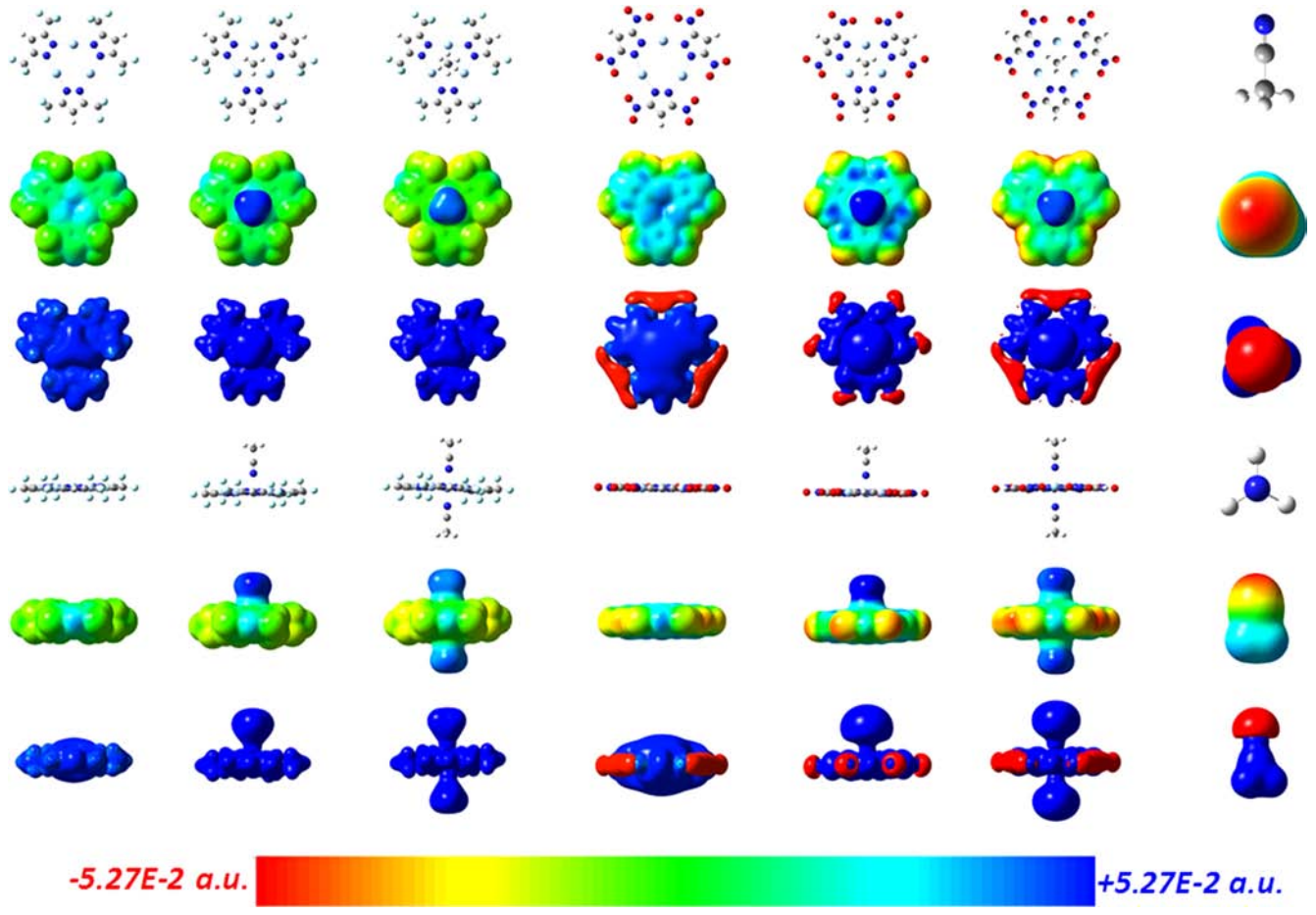

Figure 11. Illustration of quadrupole–dipole interactions involving the [Ag(3,5-$(CF_3)_2$pz)]$_3$ or [Ag(3,5-$(NO_2)_2$pz)]$_3$ trimers and acetonitrile using M06/CEP-31G(d). MEP surfaces are plotted in two manners, either mapped on electron density surfaces (rainbow plots with the color scale shown; isodensity = 0.0004) or positive (blue) and negative (red) regions in space (range = ±2.2 au; isodensity = 0.02). Atomic color code in the molecular structures: Ag, light-blue, larger spheres; C, gray; N, blue; O, red; H, white; F, light-blue, smaller spheres.

dx.doi.org/10.1021/ic401948p | *Inorg. Chem.* 2013, 52, 14124–14137

Table 8. Summary of Energetic and Structural Parameters (B3LYP and M06/CEP-31G(d)) Associated with the Quadrupole–Dipole Interaction of $[Ag(3,5\text{-}(NO_2)_2pz)]_3$ or $[Ag(3,5\text{-}(CF_3)_2pz)]_3$ with CO or CH_3CN

		B3LYP/CEP-31G(d)				M06/CEP-31G(d)			
		1CO	2CO	$1CH_3CN$	$2CH_3CN$	1CO	2CO	$1CH_3CN$	$2CH_3CN$
$[Ag(3,5\text{-}(NO_2)_2pz)]_3$	ΔE (kcal mol^{-1})	−0.66	−1.44	−8.48	−15.88	−5.81	−11.65	−13.27	−26.86
	Ag···C or Ag···N (Å)	3.67	3.67	2.97	3.03	2.94	2.95	2.90	2.87
$[Ag(3,5\text{-}(CF_3)_2pz)]_3$	ΔE (kcal mol^{-1})	−0.98	−1.98	−8.30	−15.95	−5.25	−10.69	−13.70	−30.65
	Ag···C or Ag···N(Å)	3.67	3.67	3.03	2.99	3.02	2.95	2.85	2.88

respectively. The Q_{zz} value is larger than the largest quadrupole moment tensor for CO_2 (Q_{xx} = 20 D Å),[42a] and the comparison is even more stark versus benzene or hexafluorobenzene (Q_{zz} = −8.3 and 9.4, respectively, according to literature RHF/6-31G**//S-VWN/DZVP simulations,[42b] and −5.85 and 5.69, respectively, according to our own calculations with the same method/basis set combination we used for the cyclotrimers herein). These comparisons accentuate the extremely polarizable character of the nine-membered macrometallocyclic ring compared to a linear triatomic molecule or a much smaller benzene ring. Thus, strong quadrupole–dipole interactions exist between the $[Ag(3,5\text{-}(NO_2)_2pz)]_3$ cyclotrimer, on the one hand, and the lone pair of acetonitrile (μ = 3.92 D),[43] on the other hand, as depicted in Figure 11.

For $[Ag(3,5\text{-}(CF_3)_2pz)]_3$, binding energies of 8.3 and 16.0 kcal mol^{-1} were found for one and two acetonitrile molecules, respectively, using B3LYP/CEP-31G(d), while analogous values using M06/CEP-31G(d) were 13.7 and 30.6 kcal mol^{-1}, respectively. These values are rather similar to the binding energies of $[Ag(3,5\text{-}(NO_2)_2pz)]_3$ to one and two acetonitrile molecules (Table 8). However, the nonvanishing quadrupole moment tensors (field-independent basis) are −4.4, −4.4, and 8.89 D Å, representing Q_{xx}, Q_{yy}, and Q_{zz}, respectively, which are significantly lower than the analogous values for trimer **1**. MEP plots also manifest a rather strong π-acidic behavior of this $[Ag(3,5\text{-}(CF_3)_2pz)]_3$ cyclotrimer **2**, suggesting that it should exhibit somewhat less strong quadrupole–dipole interactions with acetonitrile (three leftmost traces in Figure 11) in a manner akin to those predicted for **1**. However, the MEP surfaces show greater polarizability for the model **1**, suggested by the blue and turquoise MEP regions in the metallocyclic ring surface as opposed to the turquoise and green regions for the model **2**. Thus, both the Q_{zz} quadrupole moment tensor values and MEP surfaces offer evidence in support of the experimental finding regarding isolation of an acetonitrile adduct with $[Ag(3,5\text{-}(NO_2)_2pz)]_3$ but not $[Ag(3,5\text{-}(CF_3)_2pz)]_3$.

Figure 12 compares the electrostatic interaction energy with a positive point charge normal to the plane of both trimers; this energy is a quantitative parameter of the π-acid/base strength, as some of us prescribed earlier.[6] While the π-acidity is actually weaker for **1** versus **2** at very short distances below 2 Å from the centroid of the macrometallocycle according to Figure 12, the trend reverses above that distance such that **1** becomes a stronger π-acid by ∼4–5 kcal mol^{-1} near the bonding region with 2.5–3.5 Å (the distance range of interaction of the trimer with a Lewis base). Perhaps more importantly, the PCA remains higher for **1** than **2** by ∼3–4 kcal mol^{-1} even at very long distances of 6–10 Å, where the magnitude remains significant for **1** but vanishes for **2**. This PCA result is consistent with the polarizability being rather significantly higher for **1** according to the aforementioned quadrupole moment tensor values and the MEP profiles in Figure 11. Hence, the three effects (positive point charge calculations, quadrupole moment, and MEP profiles) corroborate to suggest that not only will a Lewis-basic molecule be more attracted to **1** than **2** but it will *diffuse* faster toward **1** than toward **2** because it will "feel" the positively charged regions of the trimer even at longer distances. The greater PCA for **1** is consistent with well-known substituent effects in physical organic chemistry because the σ_m and σ_p Hammet coefficients are 0.71 and 0.78 for NO_2 versus 0.43 and 0.54 for CF_3, albeit those values pertain to benzene substitution.[44]

Table 8 summarizes the bonding calculations of both CH_3CN and CO to **1** and **2** single molecules. While these data qualitatively confirm

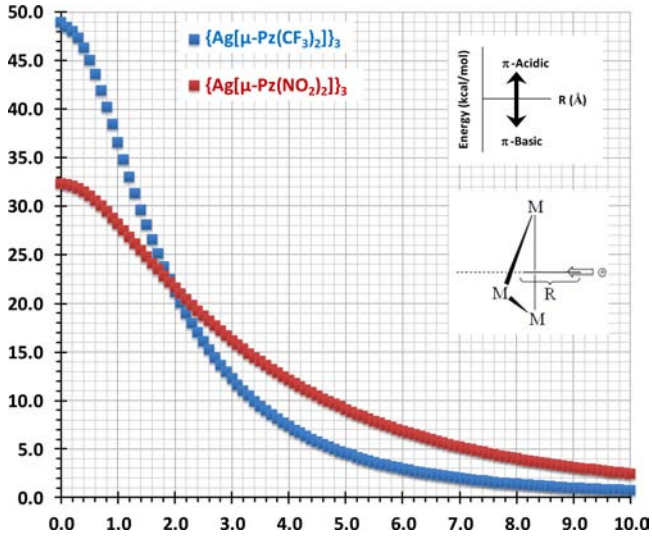

Figure 12. Electrostatic interaction energy between the $[Ag(3,5\text{-}(CF_3)_2pz)]_3$ and $[Ag(3,5\text{-}(NO_2)_2pz)]_3$ trimers with a positive point charge using M06/CEP-31G(d). The positive values indicate repulsion interaction commensurate with the MEP simulations, suggesting π-acidity, as shown in Figure 11.

the experimental findings of adsorption of CH_3CN to $[Ag(3,5\text{-}(NO_2)_2pz)]_3$ contrasted with no adduct formation between CO and either trimer, it is surprising that the computations predicted slightly stronger acetonitrile bonding to $[Ag(3,5\text{-}(CF_3)_2pz)]_3$ versus $[Ag(3,5\text{-}(NO_2)_2pz)]_3$ given the opposite experimental result showing no evidence found for the coordination of acetonitrile or other Lewis-basic solvent molecules to $[Ag(3,5\text{-}(CF_3)_2pz)]_3$ (vide supra). We attribute this anomaly to be partly due to the aforementioned diffusion argument based on electrostatic considerations, in addition to solid-state packing effects addressed in the next section.

Argentophilic Interactions. In order to gain additional insight to unravel the origin of the apparent contradiction between electrostatic and thermodynamic considerations for bonding of Lewis bases to trimer **2** versus **1**, we assess the bonding in the dimer-of-trimer model $\{[Ag(3,5\text{-}(CF_3)_2pz)]_3\}_2$. The B3LYP method does not account for metallophilic interactions, as is known for this and most prototypical hybrid DFT functionals;[45] hence, the computed dimer-of-trimer binding energy of only 2 kcal mol^{-1} (intertrimer Ag···Ag ≥ 3.96 Å vs 3.20 Å experimentally) is severely underestimated by B3LYP/CEP-31G(d) because such argentophilic interactions are expected to be much stronger.[46] Given that ab initio methods such as MP2 and CCSD(T) typically used to account for metallophilic bonding are impractical for such large dimer-of-trimer models, we used the Truhlar functional M06, which has been reported to account for weak intermolecular interactions in which dispersion forces are dominant, as it was demonstrated especially for π-stacking interactions that have similar energies to metallophilic bonding.[27,28] Thus, using M06/CEP-31G(d), the binding energy of $\{[Ag(3,5\text{-}(CF_3)_2pz)]_3\}_2$ is found to be 31.4 kcal mol^{-1}. This represents clear evidence of rather strong argentophilic bonding in the $\{[Ag(3,5\text{-}(CF_3)_2pz)]_3\}_2$ dimer-of-trimer, and the optimized structure is remarkably similar to the experimental[7] crystal structure (Figure 13 and Table 9). Therefore, the working

dx.doi.org/10.1021/ic401948p | Inorg. Chem. 2013, 52, 14124–14137

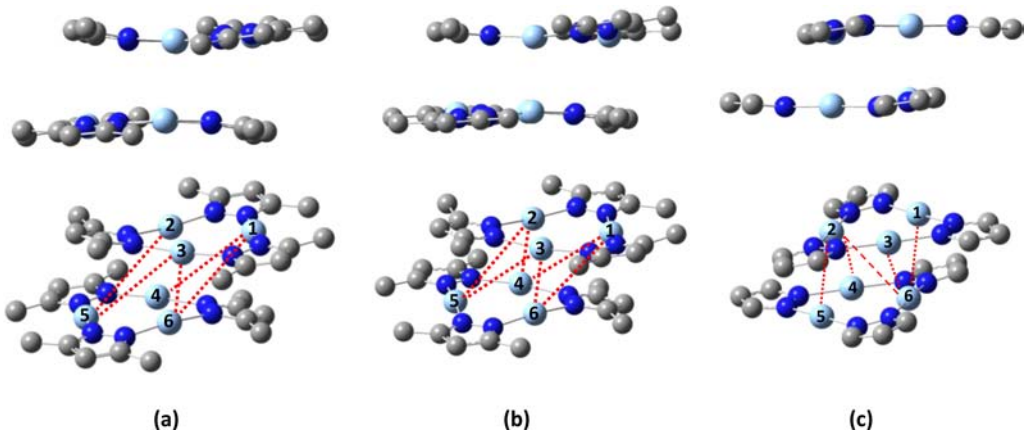

Figure 13. Illustration of the similarity between the crystal structure (a) and M06/CEP-31G(d)-optimized structure (b) of $\{[Ag(3,5\text{-}(CF_3)_2pz)]_3\}_2$, contrasted with their difference from the M06/CEP-31G(d)-optimized structure of the unsubstituted dimer-of-trimer model $\{[Ag(pz)]_3\}_2$ (c). H and F atoms were removed to simplify the view. The colors of the atoms are as follows: Ag, light blue; C, gray; N, blue.

Table 9. List of Average Ag−N and All Intratrimer and Intertrimer Ag−Ag Distances (Å) for the Crystal Structure (a) and M06/CEP-31G(d)-Optimized Structures of $\{[Ag(3,5\text{-}(CF_3)_2pz)]_3\}_2$ (b) and $\{[Ag(pz)]_3\}_2$ (c)[a]

	a	b	c
Ag−N (avg.)	2.09	2.13	2.12
Ag1−Ag2	3.50	3.52	3.50
Ag1−Ag3	3.43	3.53	3.48
Ag2−Ag3	3.55	3.65	3.51
Ag4−Ag5	3.43	3.49	3.47
Ag4−Ag6	3.54	3.67	3.50
Ag5−Ag6	3.50	3.49	3.51
Ag1−Ag4	5.44	5.18	4.41
Ag1−Ag5	7.31	6.96	5.62
Ag1−Ag6	4.76	4.54	3.38
Ag2−Ag4	3.20	3.14	3.38
Ag2−Ag5	4.76	4.65	3.38
Ag2−Ag6	4.04	4.28	3.98
Ag3−Ag4	5.42	5.28	5.62
Ag3−Ag5	5.44	4.99	4.41
Ag3−Ag6	3.20	3.11	3.38

[a]The Ag atom numbers refer to the numbering scheme in Figure 13.

hypothesis is that such strong argentophilic bonding interactions in $\{[Ag(3,5\text{-}(CF_3)_2pz)]_3\}_2$ would not allow dissociation of trimers to form adducts with 1 or 2 equiv of acetonitrile molecules given that the dimer-of-trimer dissociation energy is almost twice that of the monosolvated model. A predictive aspect of this computation to guide future experimental efforts would be to attempt crystallization from a dilute solution of $[Ag(3,5\text{-}(CF_3)_2pz)]_3$ in pure acetonitrile so as to warrant dissociated cyclotrimer units interacting with acetonitrile before they dimerize. A detailed structural comparison of the computed $\{[Ag(3,5\text{-}(CF_3)_2pz)]_3\}_2$-optimized geometry via M06/CEP-31G(d) versus the crystal structure, indicating strong resemblance, is shown in Figure 13. The intertrimer Ag−Ag bond distances, listed in Table 9, show that M06 produces similar, indeed slightly shorter, distances in comparison with those in the crystal structure. The relatively short Ag−Ag bond distances explain the strong binding energy of the dimer-of-trimer. To our knowledge, this is the first demonstration that M06 accounts for argentophilic interactions in such a large experimental model. Indeed, our simulations suggest that M06 can accurately predict the conformation of the dimer-of-trimer units of such complexes because $\{[Ag(3,5\text{-}(CF_3)_2pz)]_3\}_2$ was predicted to exhibit the same conformation as that in the crystal structure of the same compound, whereas our initial attempt to use a simplified unsubstituted $\{[Ag(pz)]_3\}_2$ model attained a different conformation in which a greater number of paired Ag atoms are engaged in intertrimer argentophilic interactions (Figure 13c). This closely packed conformation predicted for the $\{[Ag(pz)]_3\}_2$ model has yet to be attainable experimentally, likely because of the steric hindrance of substituents such as CF_3. The binding energy for the unsubstituted $\{[Ag(pz)]_3\}_2$ dimer-of-trimer model is 29.3 kcal mol^{-1}, which is slightly lower than that for CF_3-substituted dimer-of-trimer by 2.1 kcal mol^{-1}.

■ CONCLUSIONS

A new trinuclear silver(I) pyrazolate macrometallocyclic complex, $[Ag(\mu\text{-}3,5\text{-dinitropyrazolate})\text{-}N,N']_3$ (**1**), has been synthesized and characterized. The nitrated complex has been designed to possess π-acid properties akin to those reported by Tekarli et al.[6] To analyze the electrophilic nature of **1**, a comparative study with another π-acid silver metallocycle, $[Ag(\mu\text{-bis}(3,5\text{-trifluoromethyl})\text{pyrazolate})\text{-}N,N']_3$ (**2**), has also been performed. However, in contrast to **2**, compound **1** exhibits the skill to adsorb vapors of O, N, and S donor atom volatile molecules. The adsorption does not introduce a visible change in the color or in the emissive properties. Crystallographic studies of $\mathbf{1}\cdot 2CH_3CN$ indicated that the acetonitrile molecules point toward the center of the metallocycle with contacts to two of the three silver centers. According to the stoichiometry of the adducts, it is reasonable to assume that, in the case of ammonia, pyridine, or THT, a strong interaction occurs between the adsorbed molecules and the three Ag atoms. All adducts are stable in the solid state, whereas in solution a dissociative equilibrium occurs in most cases, as suggested by NMR studies. Diffusion NMR studies indicate that only the adduct $\mathbf{1}\cdot 3THT$ persists in THF-d_8 solution. The interaction between acetone, THT, NH_3, pyridine, and the silver metallocycle was proved also by large gaps between the boiling point of free molecules and the TGA delivery temperatures of the adducts. Analysis of the IR, TGA and NMR data in addition to the very low value of the BET surface (4.15 m^2 g^{-1}) of compound **1** led us to conclude that **1**/volatile adducts are held together by an appreciable chemical interaction at least in the solid state. Computational studies make a significant contribution to the understanding of the phenomenon. The M06 method gives good agreement with the experimental data both *qualitatively* and *quantitatively* compared to B3LYP. The results of positive point charge calculations,

dx.doi.org/10.1021/ic401948p | Inorg. Chem. 2013, 52, 14124−14137

polarizability, and MEP profiles suggest that the adsorption of Lewis-basic vapors occurs mainly by kinetic effects. The high versus low binding energies calculated for the adducts of **1** with CH_3CN versus CO manifest the experimental findings. On the other hand, a lack of binary adduct formation with **2** despite binding energy with CH_3CN similar to that found for **1** is explained by two computational findings: much greater polarizability of the electrostatic potential (evident from a much greater Q_{zz} quadrupole tensor coefficient and substantiated by significantly greater PCA values even at long separation from the Lewis base for **1** vs **2** models) and the high energy involved in the intertrimer Ag−Ag interaction in the dimer-of-trimer $\{[Ag(3,5\text{-}(CF_3)_2pz)]_3\}_2$ model. Finally, transformation of the highly toxic ammonia vapor initially to a strongly bound dipole−quadrupole ternary adduct **1**·3NH_3 and ultimately to the strongly bound solid salt **3** suggests excellent and novel potential for this class of macromolecular metal−organic complexes, such as **1**, toward toxic industrial chemical removal applications already known for porous organic polymers.[47]

■ ASSOCIATED CONTENT

Supporting Information

Crystal structures of compounds **1**·2CH_3CN and **3** (in CIF format; also deposited at the Cambridge Crystallographic Data Centre as CCDC 882825 and 882826) and further experimental details. This material is available free of charge via the Internet at http://pubs.acs.org.

■ AUTHOR INFORMATION

Corresponding Authors

*E-mail: rossana.galassi@unicam.it.
*E-mail: alfredo.burini@unicam.it.
*E-mail: omary@unt.edu.

Notes

The authors declare no competing financial interest.

■ ACKNOWLEDGMENTS

Dedicated to Emeritus Prof. John P. Fackler, Jr. Support by Consorzio Interuniversitario di Ricerca in Chimica dei Metalli nei Sistemi Biologici and the University of Camerino to R.G. and A.B. is gratefully acknowledged. M.A.O. acknowledges support of his group's contributions by the National Science Foundation (Grants CHE-0911690, CMMI-0963509, and CHE-0840518) and the Robert A. Welch Foundation (Grant B-1542) and also valuable feedback from Profs. Weston T. Borden, Thomas R. Cundari, and Paul S. Bagus regarding the computational modeling aspects. S.M.T. acknowledges Dr. David Hrovat for his assistance in the utilization of the computing clusters at the University of North Texas.

■ REFERENCES

(1) Dias, H. V. R.; Gamage, C. S. P. *Angew. Chem., Int. Ed.* **2007**, *46*, 2192.
(2) Lehn, J. M. *Proc. Natl. Acad. Sci. U.S.A.* **2002**, *99*, 4763.
(3) Tsipis, C. *Coord. Chem. Rev.* **2005**, *249*, 2740.
(4) (a) Yang, C.; Messerschmidt, M.; Coppens, P.; Omary, M. A. *Inorg. Chem.* **2006**, *45*, 6592. (b) Hou, L.; Wang, Y.-Y.; Wang, H.-H.; Cui, L.; Chen, P.-X.; Shi, Q.-Z. *Inorg. Chem.* **2011**, *50*, 261. (c) Okubo, T.; Anma, H.; Tanaka, N.; Himoto, K.; Seki, S.; Saeki, A.; Maekawaa, M.; Kuroda-Sowa, T. *Chem Commun.* **2013**, *49*, 4316.
(5) *Optoelectronic properties of inorganic compounds*; Roundhill, D. M., Fackler, J. P., Jr., Eds; Plenum Press: New York, 1999; p 111.
(6) Tekarli, S. M.; Cundari, T. R.; Omary, M. A. *J. Am. Chem. Soc.* **2008**, *130*, 1669.
(7) Omary, M. A.; Rawashdeh-Omary, M. A.; Gonser, M. W. A.; Elbjeirami, O.; Grimes, T.; Cundari, T. R.; Diyabalanage, H. V. K.; Gamage, C. S. P.; Dias, H. V. R. *Inorg. Chem.* **2005**, *44*, 8200.
(8) Rawashdeh-Omary, M. A.; Rashdan, M. D.; Dharanipathi, S.; Elbjerami, O.; Ramesh, P.; Dias, H. V. R. *Chem. Commun.* **2011**, *47*, 1160.
(9) Elbjeirami, O.; Rashdan, M. D.; Nesterov, V.; Rawashdeh-Omary, M. A. *Dalton Trans.* **2010**, *39*, 9465.
(10) Rawashdeh-Omary, M. A. *Comments Inorg. Chem.* **2013**, *33*, 88.
(11) (a) Peterson, G. W.; Karwacki, C. J.; Feaver, W. B.; Rossin, J. A. *Ind. Eng. Chem. Res.* **2008**, *47*, 185. (b) Petit, C.; Karwacki, C.; Peterson, G.; Bandosz, T. J. *J. Phys. Chem. C* **2007**, *111*, 12705. (c) Britt, D.; Tranchemontagne, D.; Yaghi, O. M. *Proc. Natl. Acad. Sci. U.S.A.* **2008**, *105*, 11623. (d) Glover, T.; Peterson, G. W.; Schindler, B. J.; Britt, D.; Yaghi, O. *Chem. Eng. Sci.* **2011**, *66*, 163.
(12) Canadian Centre for Occupational Health and Safety. http://www.ccohs.ca/oshanswers/chemicals/chem_profiles/ammonia.html (accessed July 18, 2013).
(13) Centers for Disease Control and Prevention. http://www.cdc.gov/niosh/idlh/7664417.html (accessed July 18, 2013).
(14) (a) Mohamed, A. A.; Chiarella, G.; Melgarejo, D.; Burini, A.; Galassi, R.; Ricci, S.; Santini, C.; Fackler, J. P., Jr. *Inorg. Chem.* **2011**, *50*, 1014. (b) Burini, A.; Bravi, R.; Fackler, J. P., Jr.; Galassi, R.; Grant, T. A.; Omary, M. A.; Pietroni, B. R.; Staples, R. J. *Inorg. Chem.* **2000**, *39*, 3158.
(15) Rawashdeh-Omary, M. A.; Omary, M. A.; Fackler, J. P., Jr.; Galassi, R.; Pietroni, B. R.; Burini, A. *J. Am. Chem. Soc.* **2001**, *123*, 9689.
(16) (a) Burini, A.; Fackler, J. P., Jr.; Galassi, R.; Grant, T. A.; Omary, M. A.; Rawashdeh-Omary, M. A.; Pietroni, B. R.; Staples, R. J. *J. Am. Chem. Soc.* **2000**, *122*, 11264. (b) Mohamed, A. A.; Galassi, R.; Papa, F.; Burini, A.; Fackler, J. P., Jr. *Inorg. Chem.* **2006**, *45*, 7770.
(17) Burini, A.; Fackler, J. P., Jr.; Galassi, R.; Macchioni, A.; Omary, M. A.; Rawashdeh-Omary, M. A.; Pietroni, B. R.; Sabatini, S.; Zuccaccia, C. *J. Am. Chem. Soc.* **2002**, *124*, 4570.
(18) Omary, M. A.; Elbejerami, O.; Gamage, C. S. P.; Sherman, K. M.; Dias, H. V. R. *Inorg. Chem.* **2009**, *48*, 1784.
(19) Janssen, J. W. A. M.; Koeners, H. J.; Kruse, C. G.; Habbaken, C. L. *J. Org. Chem.* **1973**, *38*, 1777.
(20) Dias, H. V. R.; Polach, S. A.; Wang, Z. *J. Fluorine Chem.* **2000**, *103*, 163.
(21) *Bruker APEX2*; Bruker AXS Inc.: Madison, WI, 2007.
(22) *Bruker SAINT*; Bruker AXS Inc.: Madison, WI, 2007.
(23) *Bruker SADABS*; Bruker AXS Inc.: Madison, WI, 2007.
(24) Sheldrick, G. M. SHELXTL, version 2008/3; Bruker Analytical X-ray: Madison, WI, 2008.
(25) Gregg, S. J.; Sing, K. S. W. *Adsorption, Surface Area and Porosity*; Academic Press: London, 1982.
(26) Frisch, M. J.; Trucks, G. W.; Schlegel, H. B.; Scuseria, G. E.; Robb, M. A.; Cheeseman, J. R.; Scalmani, G.; Barone, V.; Mennucci, B.; Petersson, G. A.; Nakatsuji, H.; Caricato, M.; Li, X.; Hratchian, H. P.; Izmaylov, A. F.; Bloino, J.; Zheng, G.; Sonnenberg, J. L.; Hada, M.; Ehara, M.; Toyota, K.; Fukuda, R.; Hasegawa, J.; Ishida, M.; Nakajima, T.; Honda, Y.; Kitao, O.; Nakai, H.; Vreven, T.; Montgomery, J. A., Jr.; Peralta, J. E.; Ogliaro, F.; Bearpark, M.; Heyd, J. J.; Brothers, E.; Kudin, K. N.; Staroverov, V. N.; Kobayashi, R.; Normand, J.; Raghavachari, K.; Rendell, A.; Burant, J. C.; Iyengar, S. S.; Tomasi, J.; Cossi, M.; Rega, N.; Millam, J. M.; Klene, M.; Knox, J. E.; Cross, J. B.; Bakken, V.; Adamo, C.; Jaramillo, J.; Gomperts, R.; Stratmann, R. E.; Yazyev, O.; Austin, A. J.; Cammi, R.; Pomelli, C.; Ochterski, J. W.; Martin, R. L.; Morokuma, K.; Zakrzewski, V. G.; Voth, G. A.; Salvador, P.; Dannenberg, J. J.; Dapprich, S.; Daniels, A. D.; Farkas, Ö.; Foresman, J. B.; Ortiz, J. V.; Cioslowski, J.; Fox, D. J. *Gaussian 09*, revision B.01; Gaussian, Inc.: Wallingford, CT, 2009.
(27) Zhao, Y.; Truhlar, D. G. *Theor. Chem. Acc.* **2008**, *120*, 215.
(28) Zhao, Y.; Truhlar, D. G. *Acc. Chem. Res.* **2008**, *41*, 157.
(29) Cundari, T. R.; Stevens, W. J. *J. Chem. Phys.* **1993**, *98*, 5555.

(30) Stevens, W. J.; Krauss, M.; Basch, H.; Jasien, P. G. *Can. J. Chem.* **1992**, *70*, 62.
(31) Stevens, W.; Basch, H.; Krauss, J. J. *Chem. Phys.* **1984**, *81*, 6026.
(32) Murray, H. H.; Raptis, R .G.; Fackler, J. P., Jr. *Inorg. Chem.* **1988**, *27*, 26.
(33) Galassi, R.; Burini, A.; Ricci, S.; Pellei, M.; Rigobello, M. P.; Citta, A.; Dolmella, A.; Gandin, V.; Marzano, C. *Dalton Trans.* **2012**, *41*, 5307.
(34) Maeda, M.; Nakagawa, G.; Bledermann, G. *J. Phys. Chem.* **1983**, *87*, 121.
(35) Tayyari, S. F.; Milani-Nejad, F. *Spectrochim. Acta, Part A* **2000**, *56*, 2679.
(36) (a) Dias, H. V. R.; Diyabalanage, H. V. K.; Rawashdeh-Omary, M. A.; Franzman, M. A.; Omary, M. A. *J. Am. Chem. Soc.* **2003**, *125*, 12072. (b) Dias, H. V. R.; Gamage, C. S. P.; Keitner, J.; Diyabalanage, H. V. K.; Omari, I.; Eyobo, Y.; Dias, R. N.; Roher, N.; McKinney, L.; Poth, T. *Inorg. Chem.* **2007**, *46*, 2979. (c) Yang, G.; Baran, P.; Martìnez, A. R.; Raptis, R. G. *Cryst. Growth Des.* **2013**, *13*, 264.
(37) Everett, D. H.; Haul, R. A. W.; Moscou, L.; Pierotti, R. A.; Sing, K. S. W. *Pure Appl. Chem.* **1985**, *57*, 603.
(38) Brunauer, S.; Emmett, P. H.; Teller, E. *J. Am. Chem. Soc.* **1938**, *60*, 309.
(39) (a) Rocchigiani, L.; Bellachioma, G.; Ciancaleoni, G.; Crocchianti, S.; Laganà, A.; Zuccaccia, C.; Zuccaccia, D.; Macchioni, A. *ChemPhysChem* **2010**, *11*, 3243. (b) Ciancaleoni, G.; Zuccaccia, C.; Zuccaccia, D.; Macchioni, A. In *Techniques in Inorganic Chemistry*; Fackler, J.P., Jr., Falvello, L., Eds.; CRC Press Taylor & Francis Group: Boca Raton, FL, 2010; p 129.
(40) (a) Macchioni, A.; Ciancaleoni, G.; Zuccaccia, C.; Zuccaccia, D. *Chem. Soc. Rev.* **2008**, *37*, 479. (b) Zuccaccia, D.; Macchioni, A. *Organometallics* **2005**, *24*, 3476.
(41) Perrin, F. *J. Phys. Radium* **1936**, *7*, 1.
(42) (a) Glaser, R.; Lewis, M.; Wu, Z. *J. Phys. Chem. A* **2002**, *106*, 7950. (b) Hernandez-Trujillo, J.; Vela, A. *J. Phys. Chem. A* **1996**, *100*, 6524.
(43) Steiner, P. A.; Gordy, W. *J. Mol. Spectrosc.* **1966**, *21*, 291.
(44) Hansch, C.; Leo, A.; Unger, S. H.; Kim, K. H.; Xikaitani, D.; Lien, E. J. *J. Med. Chem.* **1973**, *16*, 1207.
(45) Grimme, S. *J. Comput. Chem.* **2006**, *27*, 1787.
(46) (a) Omary, M. A.; Webb, T. R.; Assefa, Z.; Shankle, G. E.; Patterson, H. H. *Inorg. Chem.* **1998**, *37*, 1380. (b) Rawashdeh-Omary, M. A.; Omary, M. A.; Patterson, H. H. *J. Am. Chem. Soc.* **2000**, *122*, 10371. (c) Rawashdeh-Omary, M. A.; Omary, M. A.; Patterson, H. H.; Fackler, J. P., Jr. *J. Am. Chem. Soc.* **2001**, *123*, 11237.
(47) (a) Doonan, C. J.; Tranchemontagne, D. J.; Glover, T. G.; Hunt, J. R.; Yaghi, O. M. *Nat. Chem.* **2010**, *2*, 235. (b) Weston, M. H.; Peterson, G. W.; Browe, M. A.; Jones, P.; Farha, O. K.; Hupp, J. T.; Nguyen, S.-B. T. *Chem. Commun.* **2013**, *49*, 2995.